

PHENOMENA AFFECTING PENETRATION MECHANISMS
OF POLYCRYSTALLINE DIAMOND COMPACT BITS

HOSSEIN KHORSHIDIAN



Phenomena Affecting Penetration Mechanisms of Polycrystalline Diamond Compact

Bits

by

© Hossein Khorshidian

A Thesis submitted to the

School of Graduate Studies

in partial fulfillment of the requirements for the degree of

Master of Engineering

Faculty of Engineering and Applied Science

Memorial University of Newfoundland

September 2012

St. John's

Newfoundland

Dedicated to

My Parents and Samana

For their love, endless supports and encouragement

ABSTRACT

A drill setup is prepared to study the influence of borehole pressure and bit hydraulics on the performance of a drill bit.

Experimental study of bit-rock interaction shows that the negative influence of the borehole pressure on penetration mechanisms of polycrystalline diamond compact (PDC) bits, in addition to the rock strengthening under elevated borehole pressure, is the accumulation of cuttings in between the face of cutters and rock surface in the zone of penetration.

The flow of cuttings on the surface of the cutter, results in applying a confining pressure on the zone of penetration. This confinement causes a considerable rock strengthening in the zone of penetration, which increases the mechanical specific energy and reduces the rate of penetration. The value of the confinement is observed to be related to the coefficient of friction between the cutter and cuttings and the geometry of the rock-cutter interaction.

On the other hand, utilizing a bit with an appropriate jet flow significantly improves the performance of the bit. However, the experimental results indicate that there is an optimum condition for applying the hydraulic power on the bit, which yields maximum drilling efficiency.

In addition, in a simulation of a single PDC cutter-rock interaction, using the distinct element method, it has been found that there is an optimum condition for vibrations of the bit which results in the minimum energy of penetration. The optimum condition of the cutter oscillation can be defined in terms of vertical displacement

amplitude and vertical velocity amplitude of the cutter while it is moving horizontally. These parameters can be changed by adjusting inertia of the cutter with respect to the horizontal speed of the cutter.

ACKNOWLEDGEMENTS

I would like to express my deepest gratitude to my graduate supervisor, Dr. Stephen Butt, for his supervision, encouragement, and support during entire my research. Dr. Butt provided significant insight into the nature of the problem and his perceptive abilities and strategic decisions helped me to find solutions of many problems.

I dedicate my sincere thanks to Farid Arvani, project manager, for his time, consultations, extreme patience and endless support. Without his encouragement and ideas, this work would have never been completed.

Thanks to Dr. John Molgaard, Dr. James Yang and Dr. Geoff Rideout for their assistance in the design of experimental components and scientific supports.

I would like to thank the Atlantic Canada Opportunity Agency (AIF Contract no. 781-2636-1920044), Research and Development Corporation of Newfoundland and Labrador, Husky Energy, and Suncor Energy for funding this research over the past two years. Additionally, the financial and academic support of the Faculty of Engineering and Applied Science is graciously acknowledged.

Thanks to personnel of Technical Services at Memorial University of Newfoundland, especially Ron Monks, for their supports in the fabrication and accomplishment of the experimental setup.

Thanks to Brady Mining Company for providing the PDC bits for this research.

Table of Contents

Dedication	ii
ABSTRACT	iii
ACKNOWLEDGEMENTS	v
Table of Contents	vi
List of Tables	ix
List of Figures	x
List of Symbols, Nomenclature or Abbreviations	xv
List of Appendices	xviii
Notes on Units of Dimensions	1
1. Introduction	2
1.1. Importance of Drilling	2
1.2. Statement of Problem	4
1.3. Strategies for Solution	5
2. Background of Drilling Research	6
2.1. General Principles of Drilling	6
2.2. Effect of Borehole Pressures on Drilling Responses	13
2.3. Effect of Bottom-hole cleaning on Drilling Response	24
2.4. Effect of Vibrations on Drilling Responses	36

2.5. Simulation of Rock-cutter Interaction Using Distinct Element Method.....	37
3. Design and Fabrication of Test Equipment.....	38
3.1. Fabrication of Drill Setup	38
3.1.1. Rotary System	40
3.1.2. Circulation System.....	41
3.1.3. Loading System	42
3.1.4. Design of the Swivel.....	43
3.1.5. Design of the Drilling Cell.....	45
3.1.6. Sensors and Data Acquisition	49
3.1.7. Drill Bit Characteristics	50
3.1.8. Drill Bit Nozzles Characteristics.....	51
3.2. Drill Setup Characteristics	52
3.2.1. Jet Flow Characteristics	52
3.2.2. PDC Bit Characteristics	53
4. Preparation and Characteristics of rock specimen	55
4.1. Study of Grain Size Distribution.....	55
4.2. Physical Properties of the rock specimen	57
5. Design of Experiment	60
5.1. Design of Experimental Test Matrix.....	60

5.2. Experimental Test Procedure	61
5.3. Experimental Data Analysis	61
5.4. Design of Simulation Test Matrix.....	62
6. Results, Discussion and Analysis of Experiments.....	64
6.1. Results of Experiment.....	64
6.1.1. Effect of Flow Rate on Drilling Responses	68
6.1.2. Effect of BHP on Drilling Response.....	73
6.2. Mechanism of BHP in rock confinement.....	81
6.3. Mechanisms of jet flow in bottom hole cleaning.....	87
7. Results, Discussion and Analysis of Numerical Simulation *	98
7.1. Generation of Simulation Environment	98
7.2. Testing Parameters and Data Analysis.....	101
7.3. Results and Discussion of Simulation Test.....	103
8. Future Work	119
9. Conclusions.....	120
References	122
Appendix A: Petrographic Information of Aggregates in Rock Specimens	131
Appendix B: Table of Experimental Results	132

List of Tables

Table 1. Jet flow characteristics.....	53
Table 2. Result of grain size analysis.....	55
Table 3. Physical properties of the rock specimen.....	58
Table 4. DOC vs. BHP and jet parameters	69
Table 5. Pressure drop in the nozzle	89
Table 6. Results of simulation test.....	103
Table 7. Petrographic information of aggregates in rock specimen	131
Table 8. Results of experiment	133

List of Figures

Figure 1. MSE vs. cutting size (after Cook and Joughin [9])	9
Figure 2. Laboratory scale roller cone bit, drag bit and natural diamond bit.....	10
Figure 3. Micro PDC bit with two cutters.....	11
Figure 4. Penetration mechanism of a PDC cutter.....	11
Figure 5. Penetration mechanism of a roller cone bit	12
Figure 6. Hybrid of roller cone and PDC bit (after Thomson, et al. [12]).....	13
Figure 7. Influence of BHP on ROP in different rock types and drilling fluids	15
Figure 8. Rock failure via single tooth impacts under different confining pressures	16
Figure 9. Effect of the confining pressure on generation of the cutting (after Rafatian et al. [13]).....	20
Figure 10. Formation of ribbon shaped cutting material (after Wells, et al. [24]).....	23
Figure 11. Deflection of sacrificial rods with extrusion of cuttings (after Wells, et al. [24]).....	23
Figure 12. Response of ROP to increase of mechanical work in poor bit hydraulics condition	25
Figure 13. Balled up roller cone bit (after Tibbitts et al. [28])	26
Figure 14. Slant nozzle in a roller cone bit (after Cholet et al. [29]).....	27
Figure 15. PDC bit balling (after Ledgerwood and Salisbury [31])	28
Figure 16. Junk slot bit balling (after Wells et al. [24]).....	28
Figure 17. Reduction in bit performance with junk slot balling (after Wells et al. [24])	29
Figure 18. Effect of the jet parameters on ROP (after Tibbitts et al. [28]).....	31

Figure 19. Flow streams in the junk slots of a PDC bit (after Wells et al. [24])	33
Figure 20. Pressure distribution on surface in front of a nozzle	35
Figure 21. Schematic view of fabricated drill setup	38
Figure 22. Drill Setup	39
Figure 23. Rotary head.....	40
Figure 24. Circulation system	41
Figure 25. Loading system.....	42
Figure 26. Assembly of swivel	43
Figure 27. Components of swivel.....	44
Figure 28. Assembly of drilling cell	45
Figure 29. Internal components of drilling cell.....	46
Figure 30. Opened drilling cell with rock specimen	47
Figure 31. Condition of drill bit in the drilling cell	48
Figure 32. Drilling cell pressure control system	49
Figure 33. PDC cutter configurations	50
Figure 34. Nozzle configuration	51
Figure 35. Grain size distribution of aggregates used in rock specimen	56
Figure 36. Sieved aggregates are labeled as indicated in table 2.	57
Figure 37. Shear plane in a core plug after UCS test.....	58
Figure 38. Surface of the rock specimen after surface grinding	59
Figure 39. ROP vs. flow rate and BHP	65
Figure 40. MSE vs. flow rate and BHP	66

Figure 41. Balled up PDC bit.....	67
Figure 42. DOC vs. flow rate.....	70
Figure 43. DOC vs. jet impact force	70
Figure 44. DOC vs. HSI.....	71
Figure 45. Accumulation of crushed material between rock and cutter	72
Figure 46. Cleaned rock-cutter interface at high jet flow condition	73
Figure 47. Rock failure in a compressive strength test and Mohr-Coulomb failure criteria	74
Figure 48. Ascending zone and descending zone in the curve of ROP vs. flow rate	77
Figure 49. Penetration under low BHP	78
Figure 50. Accumulation of crushed material under low BHP and poor BHC	79
Figure 51. Collected cutting from filter under BHP of 2100 kPa and flow rate of 86 L/min.....	79
Figure 52. Rock-cutter interaction under elevated BHP	80
Figure 53. Flow of crushed cuttings in rock-cutter interaction.....	83
Figure 54. Reduced pressure ahead of nozzle vs. nozzle velocity.....	90
Figure 55. Reduce pressure ahead of nozzle vs. square of nozzle velocity	90
Figure 56. BHC in front of PDC cutter.....	92
Figure 57. Accumulation of powdered cuttings in the zone of penetration for the test under BHP of 1100 kPa with flow rate of 142 L/min.....	93
Figure 58. Containment of cutting flow under the tooth of a roller cone bit.....	97
Figure 59. Conditions and components of the simulation	98

Figure 60. Region of study in a simulation of single cutter-rock interaction	102
Figure 61. DOC vs. load on cutter and horizontal speed	104
Figure 62. MSE vs. load on cutter and horizontal speed	104
Figure 63. Predicted MSE in equation 23 vs. actual MSE.....	105
Figure 64. MSE vs. mass of the cutter and horizontal speed of cutter at load on cutter of 125 kN.....	106
Figure 65. Contour plot of MSE vs. mass of the cutter and horizontal speed of cutter.	107
Figure 66. Sliding of PDC cutter on the rock surface.....	107
Figure 67. Spectrum of vertical velocity at horizontal speed of 0.5 m/s and vertical load of 125 kN	109
Figure 68. Spectrum of vertical velocity at horizontal speed of 1.5 m/s and vertical load of 125 kN	109
Figure 69. Spectrum of vertical force at horizontal speed of 0.5 m/s and vertical load of 125 kN.....	110
Figure 70. Spectrum of vertical force at horizontal speed of 1.5 m/s and vertical load of 125 kN.....	110
Figure 71. Spectrum of horizontal force at horizontal speed of 0.5 m/s and vertical load of 125 kN	112
Figure 72. Spectrum of horizontal force at horizontal speed of 1.5 m/s and vertical load of 125 kN	112
Figure 73. Predicted MSE in equation 24 vs. actual MSE.....	113

Figure 74. Curve of MSE vs. horizontal velocity and peak of the axial velocity amplitude of cutter	114
Figure 75. Contour plot of MSE vs. horizontal velocity and peak of the axial velocity amplitudes	114
Figure 76. Spectrum of cutter vertical position at speed of 0.5 m/s and vertical load of 125 kN.....	115
Figure 77. Spectrum of cutter vertical position at speed of 1.5 m/s and vertical load of 125 kN.....	115
Figure 78. Normal chipping in front of PDC cutter.....	118
Figure 79. Combination of chipping and cratering after impact of PDC cutter.....	118

List of Symbols, Nomenclature or Abbreviations

A_{bit}	Area of a Hole Created by Bit
BHA	Bottom-hole assembly
BHC	Bottom-hole Cleaning
BHP	Borehole Pressure
BHS	Borehole Stress
C_d	Nozzle Discharge Coefficient
CS	Compressive Strength
DEM	Distinct Element Method
DOC	Depth of Cut
E	Energy of Fragmentation
F_j	Jet Impact Force
F_o	Normal Load on Cutter Face
F_x	Horizontal Force on Cutter
F_v	Vertical Load on Cutter
g	Gravity Acceleration
GPM	Gallons per Minute
HSI	Hydraulic Horsepower per Square Inch
K_f	Coefficient Relates the Surface Energy to Size of Fragment
LPT	Linear Potentiometer Transducer
MRR	Material Removal Rate
MSE	Mechanical Specific Energy

MSP	Mechanical Specific Power
P	Pressure
P_{bit}	Delivered Power to Bit
PDC	Polycrystalline Diamond Compact
P_c	Adjusted Borehole Pressure in Drilling Cell
P_{cf}	Confining Pressure due to Cutting Flow in front of Cutter
P_n	Injection Pressure in Nozzle
P_o	Nozzle Injection Pressure when Exhaust Pressure is Atmospheric
P_{Amb}	Ambient Pressure
P_r	Reduced Pressure in Borehole
$P(r)$	Surface Pressure at Distance of “r” from Nozzle Axis
P_s	Scavenging Pressure
Q	Flow rate
R	Distance from Nozzle Axis Where Surface Pressure Reaches to P_{Amb}
r	Radial Distance from Nozzle Axis
ROP	Rate of Penetration
S_c	Size of Crushed Rock
S_o	Original Size of Rock
TFA	Total Flow Area of Nozzles in Bit
t_1	Start Time of Study in Simulation
t_2	End Time of Study in Simulation
U	Fluid Flow Velocity

U_n	Flow velocity in Nozzle
UCS	Unconfined Compressive Strength
VFD	Variable Frequency Drive
V_h	Horizontal Velocity of Cutter
V_{rock}	Drilled Volume of Rock
V_x	Horizontal Speed of Penetration
WOB	Weight on Bit
X	Horizontal Axis
Y	Vertical Axis
Z	Vertical Distance of a Point in a Fluid Flow Line from Reference Point
β	Cutter Back-rake Angle
γ	Back-rake angle of the cutter in the chamfer
η	Drilling Efficiency
θ	Shear Plane Angle
ΔP_{bit}	Pressure Drop in Nozzles of Bit
ρ	Fluid Density
ρ_m	Drilling Fluid Density
ρ_w	Density of Water
μ_o	Friction Coefficient between bit and rock
σ_1	Principal Stress
σ_3	Confining Stress
Φ	Rock Internal Friction Angle

List of Appendices

Appendix A: Petrographic Information of Aggregates in Rock Specimens.

Appendix B: Table of Experimental Results.

Notes on Units of Dimensions

The drilling industry mainly uses imperial units for reporting the drilling parameters in both the field drilling operations and laboratory research upon American Petroleum Institute standards. In addition, SI system is used in some research. In this research SI units are mainly used for reporting the drilling parameters and response. However, for the referred literatures the original units which are used in the articles are reported. Some of these units with their conversion factors are given below.

$$1 \text{ Pa} = 0.000145 \text{ psi}$$

$$1 \text{ N} = 0.224809 \text{ lb}_f$$

$$1 \text{ L/min} = 0.264172 \text{ US gal/min}$$

$$1 \text{ m} = 3.28084 \text{ ft.} = 39.3696 \text{ in.}$$

1. Introduction

1.1. Importance of Drilling

The petroleum industry drills rocks for many purposes, e.g., wells for exploration, development and production of hydrocarbon reservoirs. Applying sufficient energy using a drilling bit on a rock, which causes chipping and cratering, is the most common rock penetration mechanism. This type of drilling is a mechanical attack on rocks and can be performed using different bits, e.g., polycrystalline diamond compact (PDC) bits, roller cone bits, impregnated bits or combinations of these bits.

Optimization, in drilling operations of oil and gas wells, is performed to reduce the cost of a drilling operation. Among all parameters which influence the drilling cost, the rate of penetration (ROP) and tripping time are the main considerations [1]. It has been observed that ROP is mainly influenced by rock specifications, bit type, weight on bit (WOB), rotary speed, bit hydraulics, drilling fluids, and borehole pressure (BHP) [2]. The tripping time is the period of time which is spent on taking a bit out of a well and running a bit down to the well bottom. Normally, a higher rate of bit wear yields more trips. Most of the current oil wells run into deeper underground formations to reach new reservoirs. Obviously, a deeper depth of drilling leads to more time for tripping.

A drilling operation at a great depth is also accompanied by higher stress on the surface of a rock which has to be drilled. It has also been observed that ROP is dramatically decreased under elevated borehole pressures [2].

Therefore, the drilling industry is trying to minimize the time of drilling by maximizing both ROP and the life of vulnerable drilling components. Despite advancement of technologies and applying optimization in drilling operations, the drilling industry still suffers from low ROP and a short life of drill bits [3].

Teale [4] defined the mechanical specific energy (MSE) as the energy required to remove a unit volume of a rock. MSE is being widely used for evaluation of drilling efficiency. Drilling efficiency is the ratio of the rock compressive strength (CS) under a specific confining pressure and the amount of energy required to drill a unit volume of that rock under the same confining pressure.

Efficient drilling is a goal for the drilling industry, which means achieving a rock failure near its strength under specific BHP. Although a drilling efficiency near 100% under elevated BHP has never been achieved, it has been observed that an optimized drilling condition can be obtained by the real time varying of the drilling input parameters [5]. Additionally, newer designs of the bit increase the efficiency of drilling operations [6].

There are several factors which cause rock penetration at depth to become more complicated than surface drilling under near atmospheric conditions. The main differences between a near surface borehole and drilling at great depth are the existence of BHP and borehole stresses (BHS) which are acting on the zone of penetration. There are also other factors which, due to interaction with the effect of BHP and BHS, influence the penetration at great depth. Among all these factors, the rock failure criteria, bit hydraulic, design of the bit, rotary speed, drilling fluids and weight on bit are known as

the most influential parameters. In many studies, these parameters have been studied as a single factor. However, neglecting the possible interaction between those parameters may call into question the outcomes of a single factor study. Therefore, obtaining practical information about drilling phenomena by studying the interactions of drilling parameters is the key for obtaining a better condition of drilling.

1.2. Statement of Problem

It is well known that rock failure under higher confining pressures needs more energy [3]. A significant reduction in the ROP and increase in MSE take place after drilling only several hundred meters [3], while the target is often around the depth of several thousand meters or more. Therefore, the main part of an oil well drilling operation is accompanied by a very low rate of advancement and high cost of operation. On the other hand, it has been observed that bottom hole cleaning (BHC) is the key for improvement of the bit performance [2]. Many reasons have been given for the positive effect of the bottom-hole scavenging. However, a comprehensive study is required to investigate the effect of the BHP, BHC and their interaction to understand how the bit hydraulics can decrease the negative effect of BHP on ROP and MSE.

Additionally, the influence of the bit axial oscillations on drilling responses is still unknown, and a comprehensive study is required to discover all the aspects of this phenomenon thoroughly.

1.3. Strategies for Solution

Both experimental and simulation approaches are used for investigation of the effect of borehole pressure, bit hydraulics, load on bit, rotary speed and bit vibration on drilling response. The experiments are conducted in conditions similar to the conditions for field drilling. ROP and MSE are the main drilling responses to study the influence of the aforementioned drilling parameters in penetration of an artificially prepared rock specimen.

In the experimental study, in addition to BHP, jet parameters, i.e., the flow rate, bit hydraulic power, nozzle velocity and jet impact force, are investigated, to discover the effect of BHC on bit performance. Other drilling parameters, such as WOB, rotary speed, bit type and nozzle configurations are kept constant for the entire experimental tests.

In addition to experimental attempts, a simulation of a single PDC cutter-rock interaction is used for studying the influence of load on cutter, speed of cut and natural vibrations of cutter on drilling responses. The study of these parameters, which is performed in the simulation environment of the distinct element method, provides useful insights for further field or laboratory investigations.

2. Background of Drilling Research

2.1. General Principles of Drilling

Penetration of a rock will be achieved by applying sufficient stress and strain to the rock. In other words, sufficient work is required for generation of cutting fragments, using a diamond or carbide cutter. Normally, a harder material is used for administration of the mechanical work. The sources of energy in a bit are the applied WOB and torque. In rotary drilling, the applied torque rotates the bit in which the bit faces a fresh rock surface and generates new cuttings. Obviously, a higher rate of fragmentation or producing larger fragment sizes yields a higher ROP.

The ROP (m/sec) can be calculated by dividing the rock material removal rate, MRR (m^3/sec), by the cross sectional area of the well created by the bit, A_{bit} , (m^2). Also, the mechanical specific energy of drilling, MSE, (J/m^3), is defined as the amount of energy (J), spent on removing a unit volume of rock, V_{rock} , (m^3). MSE is dimensionally the same as the compressive strength of the rock, CS, (N/m^2). In other words, MSE can represent the apparent strength of a rock which a bit penetrates.

Additionally, the mechanical specific power of a bit, MSP (W/m^2), is defined as the ratio of the transmitted power to the bit, P_{bit} , (W) to A_{bit} [7]. ROP can also be achieved by dividing MRR to the area of bit (Equation (1)). Furthermore, the ratio of MSP and MSE gives the ROP (Equation (2)).

$$\text{ROP} = \frac{\text{MRR}}{A_{\text{bit}}} \quad (1)$$

and

$$ROP = \frac{MSP}{MSE} \quad (2)$$

Consequently, delivering more power to a drill bit will result in a higher ROP which is desired to be maximized in most drilling operations. On the other hand, in drilling of hydrocarbon wells, transmission of power to the bit is restricted by the torsional strength of the drill string. Additionally, the material of the bit cutters, despite great improvements in strength, can only tolerate a limited amount of stress. Furthermore, drilled rock fragments have to be cleaned efficiently to prevent the bit from foundering on previous drilled materials.

In addition to ROP, the efficiency of a drilling operation, η , which is given by Equation (3), plays an important role in adjusting the drilling parameters.

$$\eta = \frac{CS}{MSE} \quad (3)$$

Equation (1) and (2) imply that under a fixed specific power of a bit, minimizing the specific energy maximizes both the drilling efficiency and ROP. Additionally, maximizing the drilling efficiency causes maximizing the life of a drill string and bit due to the lower ratio of damage of drilling facilities to a unit length of drilling operation. In other words, the total tripping time of a drilling operation will decrease. The main restrictive factors in drilling efficiency are energy lost due to friction and design of bit.

According to Rittinger, [8, 7] the specific energy of a drilling operation is inversely proportional to the size of the produced fragments. Generation of smaller particles or a bigger total surface area requires a higher amount of energy which is used for breaking the bonds between the materials of a rock. Rittinger's formula is shown by Equation (4).

$$E = K_f \left(\frac{1}{S_o} - \frac{1}{S_c} \right) \quad (4)$$

where "E" is required energy to break a unit volume of the rock from the original size of "S_o" to the crushed size of "S_c", and "K_f" is a coefficient which relates the surface energy of the fragments to their size.

Different methods of drilling produce different fragment sizes. Therefore, the amount of MSE with respect to the administered technology of drilling will be different. In the petroleum industry there are several drilling methods which are widely used for underground rock penetration. Those methods are mainly mechanical attack to the rock with assistance of hydraulics. Cook and Joughin [9] compared several drilling methods with respect to their produced fragment size and the required specific energy under atmospheric conditions. The result of this comparison is depicted in Figure 1. It can be seen that the value of specific energy decreases by the increase in the size of the produced fragment. However, in a drilling operation at great depth, regarding different conditions of penetration, the value of MSE might differ from the results for surface penetration.

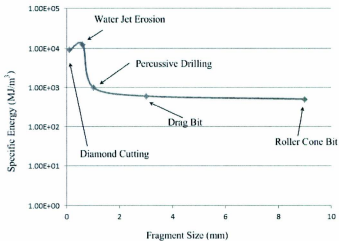


Figure 1. MSE vs. cutting size (after Cook and Joughin [9])

In the method of diamond cutting, natural diamonds are used as the cutters for generation of rock fragments, and are often embedded in an impregnated metallic matrix.

In the method of water jet erosion a high pressure jet is used for cutting. Also, abrasive contaminants can enhance the rock penetration mechanism [7]. The mechanism of percussive drilling imposes high energy blows on the rock surface. The teeth of the percussive bit are able to penetrate a rock when the pressure in teeth-rock interface becomes greater than rock compressive strength [10], and subsequent tensile splitting of the rock can occur beneath the penetrating teeth.

The roller cone bit constitutes several rollers with teeth on their surface. Applying an appropriate load on bit and rotation causes the teeth to penetrate the rock due to cratering. When a tooth applies a stress higher than rock strength on the rock surface,

cuttings will be generated [10]. Drag bits penetrate the rock with the contribution of both the applied WOB and torque. A hardened material, with a positive rake angle, causes chipping in the rock. Figure 2 shows a two cone micro roller bit, micro drag bit and micro natural diamond bit, each with a diameter of 32 mm. However, the depicted natural diamond bit has larger diamond than bits which are normally used in the method of diamond cutting

The new generation of drag bits, which came after the work of Cook and Joughin [9], is the PDC bit. The PDC bit uses very hard cutters made from polycrystalline diamond compact material for rock penetration. In most of the PDC cutters the rake angle is negative, which is called the back-rake angle (Figure 4). Figure 3 shows a micro PDC bit with two cutters.

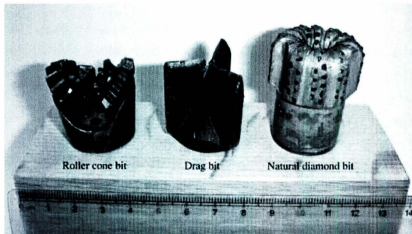


Figure 2. Laboratory scale roller cone bit, drag bit and natural diamond bit

(Courtesy of W. Maurer)



Figure 3. Micro PDC bit with two cutters

Figure 4 schematically shows how a PDC cutter generates chips and penetrates a rock. Figure 5 shows how a crater is created after the action of a tooth of a roller cone bit. These types of fragmentation can occur under the atmospheric condition of penetration.

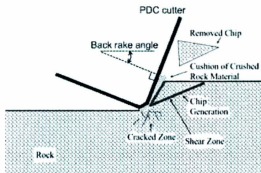


Figure 4. Penetration mechanism of a PDC cutter

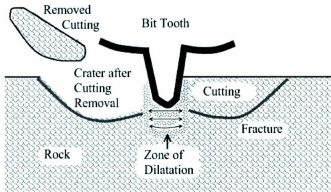


Figure 5. Penetration mechanism of a roller cone bit

Combinations of these abovementioned bits are called hybrid bits. The hybrid of the roller cone and PDC bit is presented in Figure 6. Drill bit manufacturers are trying to combine mechanisms of rock fragmentation, which are generally diamond cutting, chipping, cratering and water jets, to maximize efficiency of penetration. It is clear that removing the generated cuttings causes the bit to penetrate a new surface of a rock and prevents regrinding the previous cuttings. Also, a combination of mechanisms of chipping and cratering may result in a better drilling operation.

The performance of the hybrid bit was evaluated in different rocks at elevated borehole pressure and compared to the performance of a roller cone bit and a PDC bit. The criteria for comparison are ROP and MSE. The result of those experiments show that in the soft rocks, (Catoosa shale) the PDC bit gives the best performance, and in hard rocks, (Jasper and Gabbro) the hybrid bit obtains the best performance

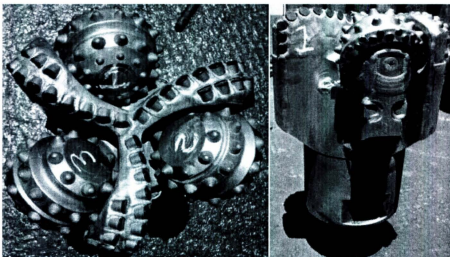


Figure 6. Hybrid of roller cone and PDC bit (after Thomson, et al. [12])

2.2. Effect of Borehole Pressures on Drilling Responses

It is well known that drilling of deep wells is operated with a lower ROP than surface drilling for the same type of formation [13]. The main difference between depth drilling and surface drilling is the stresses acting on the zone of penetration. There are several pressures around the region of penetration which may influence the drilling responses, e.g., BHP, pore pressure and the borehole stresses. Additionally, rock properties, such as internal friction, porosity, permeability and type of minerals, may interact with these above indicated pressures. Investigations have related the reduction in ROP to phenomena which are acting on the shear plane of generated chips [14]. The shear plane is the area between disintegrated rock fragments and intact rock specimen.

Studies showed that overburden pressure around the rock specimen constitutes no considerable effect on the penetration mechanism. Garnier and Van Lingen [2] and Cunningham and Eenink [15] conducted similar studies on the effect of non-fluidic borehole stresses on the ROP. In these studies, the confining and lateral pressure around a jacketed rock was varied while other drilling parameters were kept constant. No significant effect for the borehole stresses was observed. The same result was also reported by Sellami [16]. In this study, the action of a PDC bit cutter using a finite element model was analyzed. The result of the analysis was also verified by conducting experimental tests, using a single cutter test device. Sellami argued that the effect of borehole stress, in comparison to the effect of BHP, on the performance of the cutter is negligible. Therefore, BHP and pore pressure can be the influential pressures which constrain the performance of a bit in drilling operations at great depth.

Garnier and Van Lingen [2], using a drag bit with diameter of 1 ¼ inches, examined the effect of BHP on drilling responses in three different rocks. It was observed that in the permeable rocks (Obernkirchener sandstone and Vaurian limestone) change in BHP, when water is used as drilling fluid, posed no significant influence on ROP. However, increase in BHP, by using water in the drilling of a low permeable rock (Belgian limestone), and using mud in drilling of the all rocks, decreased the ROP. It was also observed that increasing BHP could decrease the ROP to a specific reduction factor; afterwards it could no longer influence the ROP. Figure 7 shows the results of the experiment for the influence of BHP on ROP. Garnier and Van Lingen also observed that increase in the rotary speed, WOB and clay content of drilling fluid produce a negative

effect on the performance of the bit. Additionally, it has been suggested that in permeable rocks, due to the existence of a smaller difference between BHP and pore pressure, the chip hold-down effect is less significant.

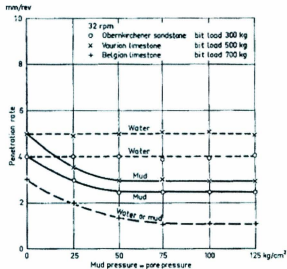


Figure 7. Influence of BHP on ROP in different rock types and drilling fluids

(after Garnier and Van Lingen [2])

The higher permeability of a rock may decrease the effect of BHP on chip hold-down by two mechanisms. Both mechanisms compensate for the pressure drop in the shear zone, which exists due to an increase in the volume of pore space. In the first mechanism, higher permeability increases the rate of pore fluid diffusion in the zone of penetration, and in the second mechanism, higher permeability causes compensation of pore pressure by an increase in invasion of drilling fluid in the zone of penetration.

Maurer [10] studied phenomena in rock failure by a single tooth which penetrates the rock via dynamic impacts under elevated hydrostatic pressure. The action of a single tooth is assumed to be proportional to the action of a tooth of a roller cone bit. Maurer argued that penetration under low BHP yields brittle failure of the rock. However, under the higher BHP, the rock failure is pseudoplastic. Figure 8 represents the rock failure under single tooth impact for the aforementioned conditions.

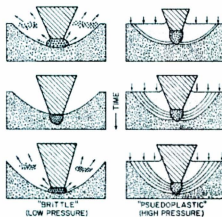


Figure 8. Rock failure via single tooth impacts under different confining pressures

(after Maurer [10])

Additionally, under the higher BHP when water and air are used as the drilling fluid, the threshold load for rock failure is equal to the atmospheric condition of penetration. However, when the rock surface is coated by an impermeable layer of mud cake the threshold load for rock failure is higher. In addition, it was reported that when water is used for raising the BHP, no significant increase in threshold load was observed,

but the volume of the produced crater was decreased with an increase in BHP by water. However, by using air as a pressurizing fluid, neither crater volume nor threshold load were affected by raising BHP.

In a similar study, Yang and Gray [17] studied the influence of effective stress on penetration mechanisms of a single tooth on two different sandstones with high and low permeability. The nominal effective stress is defined as difference in pore pressure and BHP. The result of the tests showed that in the case of using Soltrol, which is an isoparaffin solvent, as a pressuring fluid, despite zero nominal effective stress, both rocks tend to fail in a ductile manner. However, in case of using liquid nitrogen, the more permeable rock fails in a brittle manner, and the less permeable rock fails in a brittle to ductile transition manner.

Black et al. [18] examined the effect of mud filtration on ROP. This study was conducted to observe the influence of the rate of drilling fluids filtration on reduction of the nominal effective stress and consequently, the increase in ROP due to a lower chip hold-down condition. A significant relation between the rate of filtration while drilling and ROP was suggested.

On the other hand, Cunningham and Eenink [15], by evaluating responses of a drilling experiment on two different sandstones with different permeability, suggested that rock permeability poses no significant effect on drilling response under elevated BHP.

Peltier and Atkinson [19] theoretically evaluated the influence of a low permeable skin layer on the differential pressure between BHP and pore pressure. The skin zone is a

layer for which the permeability, due to plastering of fine particles, is damaged. In this study it was argued that in highly permeable rocks, despite what is expected for the existence of a low differential pressure, because of a higher initial rate of filtration, the fine particles plug the filtrate flow paths. Therefore, a very low permeable skin will be generated. The skin layer coats the surface of the rock between actions of the bit teeth and causes a lower volume of drilling fluids to reach the pore space. Consequently, higher rock permeability may yield a higher chip hold-down condition.

Peltier and Atkinson [19] also showed that for a rock with a permeability of less than 0.0001 mD, e.g. concrete, when ROP becomes more than 3.6 m/hr., the porous medium in the region underneath the bit could not be invaded by drilling fluid pressure. Also, for a rock with a permeability of less than 0.001 mD, e.g. Carthage marble, the above mentioned phenomenon would occur at an ROP of higher than 36 m/hr. Based on the aforementioned hypothesis, a high ROP, by restricting the time of filtration diffusion, prevents transmission of BHP to the pore space underneath the bit. Therefore, a bit will face with a harder rock at a higher ROP.

In a theoretical study Detournay and Atkinson [20] performed an analysis on the mechanism of the chip-hold down phenomenon. In this analysis the mass balance of pore fluid diffusion in the shear zone is considered for a rock with a porosity of 10% and a permeability of less than 10 nD and a shear plane angle of 15°-45°. In such a rock, if the PDC cutter penetrates the rock with a cutting velocity of 1 m/s and a depth of cut of 1 mm, and if the pore fluid viscosity is 1 cp, and fluid compressibility factor is $5 \times 10^{-4} \text{ MPa}^{-1}$, and if the change in porosity due to the shear is only 1%, a differential pressure of

200 MPa is generated in the shear plane. This pressure is much greater than existing BHP in drilling operations. Therefore, a vacuum occurs in the shear zone, and the generated chip will be held-down by the force which would be applied by the entire BHP on the cuttings' surface area. In other words, for the abovementioned condition, pore pressure could no longer have any influence on penetration. In this theory it is assumed that there is no flow of drilling fluids filtrate into the shear zone. In addition, certainty of the performed analysis was restricted to only low permeable rocks such as shale.

Detourmay and Tan [21] examined the above indicated theoretical findings by penetrating several rocks under a fixed depth of cut using a single cutter test device. They found that the specific energy of penetration is only dependent on the borehole pressure, and pore pressure plays no role in the amount of specific energy. In addition, they discovered that the shear angle of rock fragments in front of the cutter is very close to the rock shear angle in an UCS failure test. Also, the shear angle interacts with the influence of the borehole pressure in drilling specific energy.

Gray et al. [22] also, using a milled tooth roller cone bit, examined the effect of pore pressure by drilling two different shales of the North Sea area. The same result of ineffectiveness of the pore pressure on drilling response was reported.

In a single cutter test Rafatian et al. [13], using a PDC cutter, studied the effect of BHP on drilling efficiency. In this study, through penetration in Indiana limestone and Carthage limestone, it is shown that only 100 psi increase in BHP for Indiana limestone, and 150 psi for Carthage limestone, could decrease drilling efficiency by 50%. In these experiments, the pore pressure was opened to the atmosphere, and the radial confining

stress around the rock was equal to BHP. Rafatian also varied the fluid viscosity and rock permeability in several tests, which yielded no significant effect on the performance of the cutter. Rafatian argued that the reduction in drilling efficiency is related to an increase of friction in the sheared zone due to the chip-hold down phenomenon. In this investigation, due to the characteristics of the test set up, no study was performed on the effect of drilling fluid circulation and cutter cleaning. Additionally, the data of the penetration are related to a low depth of penetration which due to an unsteady state regime of rock-bit interaction may bring the results into question. Figure 9 schematically shows that the generation of cutting is influenced by pressurized borehole conditions. The cuttings under a confining pressure of 150 psi tend to move upward and parallel with the face of the PDC cutter.

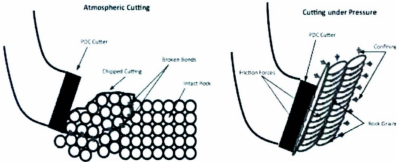


Figure 9. Effect of the confining pressure on generation of the cutting (after Rafatian et al. [13])

The other parameter which may interact with borehole pressure is friction between generated fragments. Van Lingen [23], using a 31.75 mm drag bit, conducted a drilling test in an unconsolidated sandstone. A very high ROP under atmospheric conditions of 20

drilling was achieved. Also, under BHP of 50 kg/cm^2 (4.9 MPa), the DOC was measured 7mm. However, under BHP of 100 kg/cm^2 (9.8 MPa), DOC was measured at only 2.5 mm. This reduction was justified by the concept of the increase in the friction between sand particles and rock strengthening under confining pressure.

Maurer [10] also conducted a test on powdered sands under elevated BHP in which a single tooth penetrates the bulk of sand. The sands' surface was coated with a layer of impermeable mud cake, and a pressure was applied on top of the sand while the pressure inside the sand matrix was opened to the atmosphere. The required force for 0.15 inches penetration into the powdered sand from near zero under atmospheric pressure was increased to 3,500 lb under BHP of 10,000 psi. Maurer argued that for the powdered sand, cohesive and tensile strength at the atmospheric condition is zero, and the threshold load increment occurred due to friction between sand particles, which is sufficient to change brittle cratering to pseudoplastic failure.

In a similar attempt, Cunningham and Eenink [15], using a drag bit with diameter of $1 \frac{1}{4}$ inch, examined the effect of differential pressure on drilling responses in loose sand. In this experiment it was observed that ROP of 15 ft. /hr., which was achieved under BHP of 1000 psi, decreased to below 1ft. /hr. under BHP of 5000 psi. This value of ROP in drilling loose sand under BHP of 5000 psi is close to the ROP of drilling in an Indiana limestone with same applied drilling conditions. These results illustrate the impact of the rocks' internal friction on drilling response under elevated BHP.

In shear failure of rock under compression [14], Maurer showed that an increase in the normal force to the shear plane of a failed rock in addition to increase in the friction

may increase the coefficient of the friction. It has been also suggested that brittle failure of a rock will be changed to ductile failure when a high normal force causes large increase of friction in the shear plane. The ductile failure causes most of the rock fragments to exist in a deformed shape after failure of the bonds between the particles.

The ductile failure of a rock can be observed in drilling under high BHP. Wells et al. [24] attached several small rods on top of cutters in a PDC bit, perpendicular to the cutters' face, for measuring the strength of ribbon shaped cuttings which are being generated in the drilling of Catoosa shale under elevated borehole pressure. Formation of ribbon shaped cutting material is shown in Figure 10. Results of rod deflections imply that the strength of the generated cutting material in drilling of Catoosa shale with UCS of 6000 psi, under BHP of 5400 psi should be greater than 9000 psi. The deflections of rods are also shown in Figure 11.



Figure 10. Formation of ribbon shaped cutting material (after Wells, et al. [24])

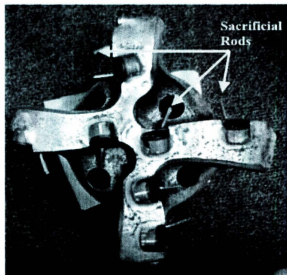


Figure 11. Deflection of sacrificial rods with extrusion of cuttings (after Wells, et al. [24])

2.3. Effect of Bottom-hole cleaning on Drilling Response

The use of fluid circulation is necessary for all drilling operation. There are many reasons for utilizing a drilling unit with an appropriate circulation system [11]. While a drilling bit is generating fragments, fluid flow is required for removing the cuttings, which are being generated by the bit. Moreover, these cuttings should be carried to the surface from depth. Removal of the generated cuttings is called bottom-hole cleaning. The drilling fluids also cool the bit for a lower rate of bit wear [25]. Furthermore, in deep well drilling, the use of drilling fluids for borehole stability and well control purposes is mandatory. However, the circulation of drilling fluids is known as one of the significant factors for achieving a higher ROP.

Maurer [26] in “Perfect-Cleaning Theory of Rotary Drilling” discussed the effect of BHC on ROP. In this study, it was argued that ROP is a function of bit rotary speed, WOB, bit diameter and the rock strength. However in drilling with high WOB and rotary speed, the increasing trend of ROP will be stopped. The aforementioned phenomena are depicted in Figure 12. Maurer theorized that this phenomenon is due to a shortage in BHC which causes bit floundering in previous crushed rock cuttings. The theory of floundering or re-drilling of cuttings, due to lack of cleaning, can be true for a high bit rotary speed and WOB. However, further study is required to discover mechanisms of BHC for improvement of bit performance.

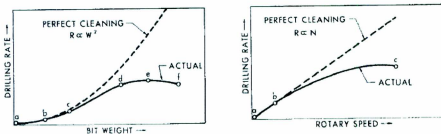


Figure 12. Response of ROP to increase of mechanical work in poor bit hydraulics condition

(after Maurer [26])

Garner [27] studied the performance of a single diamond cutter in the penetration of shale and limestone, under elevated BHP with no fluid circulation. The results of this study showed that the volume of the cut was dramatically reduced by an increase in BHP. In addition, fine powdered fragments were observed in the groove created by penetration.

Garnier and Van Lingen [2] also studied the effect of BHC on drilling tests under elevated BHP. It has been observed that fine particles of crushed rock and the clay content of mud pose a significant effect on ROP of a roller cone bit. Garnier and Van Lingen argued that the fine particles play a significant role in damaging the rock permeability underneath the bit. This phenomenon was called bottom-hole balling due to bit plastering. Additionally, it was observed that crushed particles could stick between the teeth of the bit and decrease bit efficiency. This condition is called bit balling. Figure 13 presents a balled up roller cone bit which is the result of a low bit hydraulic power in drilling of Mancos shale.



Figure 13. Balled up roller cone bit (after Tibbitts et al. [28])

Garnier and Van Lingen argued that bit balling and bottom-hole plastering significantly reduce ROP. In this study, it was suggested that a high circulation flow rate not only increases the carrying capacity of generated cuttings but also mitigates the ROP by cleaning the aforementioned fine particles. Further investigations by Van Lingen [23] showed that in addition to the flow rate, the position of nozzles near the bottom-hole and using a smaller nozzle size can enhance ROP.

The advantage of slant nozzles near the cones of the bit and bottom-hole was also suggested by Cholet et al. [29]. Figure 14 schematically shows how the slant nozzle yields a better cleaning condition.

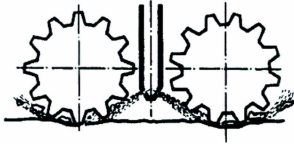


Figure 14. Slant nozzle in a roller cone bit (after Cholet et al. [29])

In a similar study, Feenstra and Leeuwen [30] argued that in soft and medium strength rocks, ROP is hampered by bit balling. They also observed that bit balling can be more severe under greater WOB. Furthermore, they suggested that the bit balling, which may drop the ROP by 50%, can be eliminated by applying high velocity jet flow.

Bit balling is also observed for PDC bits when the hydraulic power is low. This phenomenon is more pronounced in the drilling of soft rock such as Catoosa shale. Ledgerwood and Salisbury [31] suggested that the sticky cutting material on the bit and bottom-hole can be generated when the fluid flow is insufficient to carry the cuttings. In such a condition, the crushed material will be compacted between the bit and rock. Consequently, those materials, due to compaction and losing water, will create a stuck mass in the zone of penetration. Several examples of micro PDC bit balling are presented in Figure 15.

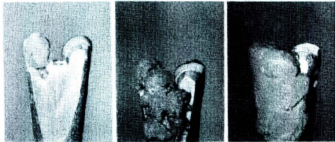


Figure 15. PDC bit balling (after Ledgerwood and Salisbury [31])

Wells et al. [24], in drilling of Catoosa shale with a PDC bit, observed that an increase in WOB under a constant bit hydraulic horsepower causes the balling of junk slots. This phenomenon is shown in Figure 16. This indicated condition of the bit may result in a significant drop in ROP and increase in the torque of bit. Figure 17 shows how bit balling constrains the performance of PDC bits.

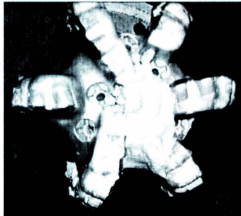


Figure 16. Junk slot bit balling (after Wells et al. [24])

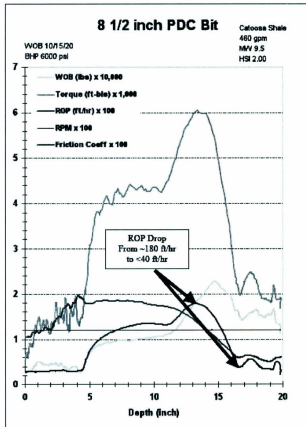


Figure 17. Reduction in bit performance with junk slot balling (after Wells et al. [24])

In the drilling industry the hydraulic power of a bit is often expressed in terms of the amount of hydraulic horse power per unit area of bit (HSI). The hydraulic horse power of a bit can be calculated by Equation (5).

$$\text{HHP} = \frac{\Delta P_{\text{bit}} \times Q}{1714} \quad (5)$$

Where ΔP_{bit} is the pressure drop of the bit nozzle in psi, and Q is the flow rate in GPM.

The bit pressure drop is also dependent on the flow rate and total flow area of the nozzles (TFA). Equation (6) shows the relation between bit pressure drop and the parameters indicated above.

$$\Delta P_{bit} = \frac{\rho_m \times Q^2}{12032 \times C_d^2 \times TFA^2} \quad (6)$$

where the C_d is the nozzle discharge coefficient, TFA is the flow area in in.^2 and ρ_m is the mud density in lb/US gal.

Therefore, for a specific drilling fluid, HSI of a bit is dependent on two parameters which are the flow rate and TFA. The relation among HSI, flow rate and TFA is given below.

$$HSI \propto \frac{Q^3}{TFA^2} \quad (7)$$

Thus, decreasing TFA under a fixed flow rate causes a higher pressure drop in the nozzle, higher jet velocity and greater HSI. Also, increasing the flow rate under a fixed TFA of the nozzles produces the same results.

Tibbitts et al. [28] studied the effect of both TFA and the flow rate on ROP of different roller cone bits in the drilling of shale. It has been observed that ROP is

generally higher at higher bit HSI. However, there is an optimized TFA with respect to the applied hydraulic horsepower. The optimized TFA at higher HSI was found to be smaller than the optimum TFA at lower HSI. The result of this study is shown in Figure 18.

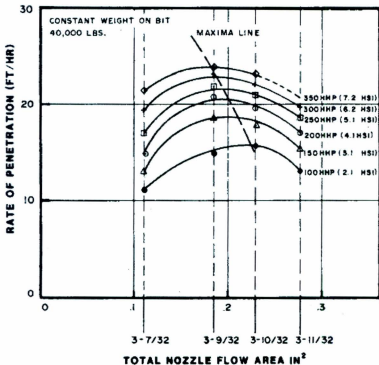


Figure 18. Effect of the jet parameters on ROP (after Tibbitts et al. [28])

Decreasing the nozzle diameter yields higher jet velocity and impact force. Equation (8) gives the jet impact force in SI units.

$$F_j = C_d \times Q \times \sqrt{\Delta P_{bit} \times \rho_m} \quad (8)$$

Maximizing the jet impact force is one of the targets for bit hydraulic optimization [11]. A jet with a higher impact force, in addition to cleaning the generated cutting material, may result in a further scavenging of the aforementioned fine particles which cause the bottom-hole balling.

Rabia [32] discussed that, for PDC bit hydraulics, there are three regimes for ROP vs. HSI. In the first regime, minimum flow rate is required for removing the generated cutting and to prevent bit balling. The estimated HSI for this regime is 2. In this regime the jet plays a small role in bottom-hole scavenging. In the second regime, which is accompanied with a higher flow rate, bit hydraulic horse power could be effective as well as flow rate (HSI between 2 and 4). In other words, increasing the bit pressure drop, by reducing the TFA under a fixed flow rate or by increasing the flow rate under a fixed TFA, yields improvement in the bit performance. In the third regime, which is HSI of higher than 4, ROP is more responsive to the mechanical work of the bit. Therefore, a minimum HSI is required for utilizing the bit's mechanical work for the enhancement of the ROP. The above indicated study [25], which was performed on Gulf Coast shale, neglects the relation of BHC and borehole pressure.

On the other hand, in a recent investigation [24] of the influence of the bit hydraulic on ROP of an IADC M323 PDC bit, it has been shown that the HSI poses a significant influence on ROP only in soft rocks such as Catoosa shale. However, in harder rocks, such as Mancos shale and Carthage limestone, neither the HSI nor the flow rate makes

any significant difference to ROP. However, further analysis illustrates that the fluid velocity adjacent to the face of PDC cutters can better correlate the ROP to the bit hydraulic than HSI. Figure 19 demonstrates a fluid flow in junk slots of a PDC bit which was achieved by using a computational fluid dynamics simulation.

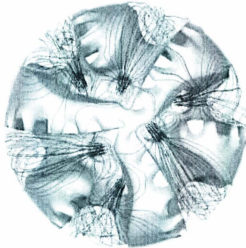


Figure 19. Flow streams in the junk slots of a PDC bit (after Wells et al. [24])

The reason for a marginal influence of the jet impact force on ROP of the PDC bit in comparison to roller cone bits and micro bits can be the difference in positions of the nozzles with respect to zones of cuttings generation. In a PDC bit, nozzles are located where the fluid flow swipes all the PDC cutters, which prevents the bit balling. However, in roller cone bits, both the formation and teeth are targeted by the jet nozzles and encounter the jet impact force.

McLean [33] experimentally found that for a roller cone bit, the fluid velocity across the bottom-hole and beneath the bit is maximized when the jet impact force is maximized. Additionally, Eckel [34] suggested that the performance of a micro bit is also directly linked to the jet impact force.

Utilizing a bit with high velocity jets, in addition to having an influence on the ROP, is also known to be a primary parameter for achieving a higher efficiency of penetration. Armenta [35] suggested that a considerable improvement in drilling efficiency can be achieved by applying a high pressure jet on the bit. Furthermore, in many investigations it is observed that high pressure jets cause reduction in the force components acting on a bit [7].

Tutluoglu [7], judging from the results of a single cutter test which penetrates a rock under atmospheric conditions with a fixed DOC, suggested that the main restricting factor in the performance of a cutter is the accumulation of crushed particles in front of the cutter. In addition, it was argued that cleaning the zone of crushed particles, by reducing the horizontal force on the cutter, dramatically improves the specific energy of penetration.

Leach and Walker [36] argued that there is a critical value for a jet impact force below which no damage can be created on a rock surface, but that high pressure jets can remove the generated particles. However, Tutluoglu [7] argued that an improvement in the penetration mechanism, after applying a certain amount of jet hydraulic power, can no longer be achieved. Speer [37] also postulated that the improvement in penetration by hydraulic power is restricted to cleaning the entire generated cuttings material, which is

called perfect BHC. Therefore, the role bit hydraulics may be limited only to the cleaning of drilled materials and not contributing in rock failure.

Leach and Walker [36] characterized the performance of a nozzle with respect to the pressure distribution on a surface at the right angle to the nozzle axis with a specific stand-off distance. Above indicated parameters are schematically depicted in Figure 20.

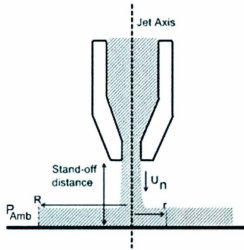


Figure 20. Pressure distribution on surface in front of a nozzle

Equation (9) can be used to estimate the surface pressure in SI units.

$$P(r) = P_0 + \rho_w \times U^2 \times \left(1 - 3 \left(\frac{r}{R} \right)^2 + 2 \left(\frac{r}{R} \right)^3 \right) \quad (9)$$

where $P(r)$ is the pressure in points of the surface which are located with a radial distance of “ r ” from the jet axis. P_{Amb} is the ambient pressure, and ‘ R ’ is the distance from the jet axis where the surface pressure becomes equal to the ambient pressure. It is also argued

that for a good configuration of a nozzle, the injection pressure can be applied effectively on a surface with a stand-off distance of less than 100 times greater than the nozzle diameter. Additionally, it was reported that the surface pressure, in a region of approximately 2.6 jet radii, is considerably greater than the ambient pressure and can be 80% of the nozzle inlet pressure.

2.4. Effect of Vibrations on Drilling Responses

Vertical oscillations of the bit and drill string during drilling operations, which is mainly due to forces acting on bits, can influence the efficiency of penetration [38]. Study of a model of a single cutter-rock interaction can provide detail information about effect of drilling parameters such as load on cutter, cutter mass and speed, on drilling responses e.g., cutter force components, vertical vibrations, DOC and MSE.

The cutting action is the result of applying a sufficient load on a cutter and moving it in the direction of the cut. Due to the discontinuous process of chips generation, the force components acting on cutter oscillate [38] and cause vibration in the cutter.

Dunayevsky et al. [39] argued that the dynamic components of the force are primarily the result of the bit-formation interaction. Also, Dubinsky et al. [40] suggested that dynamic forces, which are the result of bit and string interaction with rock, cause vibration in the bit. In addition it was argued that the drill string and bit vibrations are linked to the vertical stiffness of the pipe and the mass of the bottom-hole assembly. Fluctuations of forces in the direction of cut can result in bit stick-slip which in addition to increase in the risk of bottom-hole assembly (BHA) failure, yield reduction in the ROP [41].

In another study of bits vibration, Richard et al. [42] showed that torsional and vertical vibrations of a PDC bit are coupled. Additionally, it has been argued that the bit oscillations could be controlled by changing the WOB and velocity.

Improvements of bit performance and BHA life have been observed when a downhole thruster is used in the BHA [43]. A downhole thruster is a tool which converts the differential pressure of the drilling fluids between the inside of the drill string and annular space to load on bit. Therefore, by using this tool it is possible to adjust the inertia of the drill collars and load on bit independently. Additionally, improvement of the bit performance has been observed in PDC and roller cone hybrid bit [6], which due to action of the roller cones has higher axial vibrations in drilling of hard rocks.

Results of the previous studies showed significant effects of the dynamics of bit motion on the penetration mechanism; however, there is still no clear insight about effects of the vibration on the penetration mechanism.

2.5. Simulation of Rock-cutter Interaction Using Distinct Element Method.

In early attempts of rock-cutter simulation using distinct element method (DEM), it has been observed that DEM is able to demonstrate phenomena affecting penetration mechanism of a single cutter such as, transition from brittle to ductile at high pressure conditions [44], generation of ribbon shape cutting in plastic deformation at pressurized cutting condition [45] and generation of the different fractures and cutting shapes under different load on cutter functions [38]. Those phenomena showed an acceptable agreement of the simulation of a rock-cutter interaction, using DEM, with real experimental reports.

3. Design and Fabrication of Test Equipment

3.1. Fabrication of Drill Setup

An existing laboratory drill rig setup, which includes a rotary head and loading system, which was designed for atmospheric drilling condition, was modified for simulation of downhole drilling conditions. The modified drill setup fulfills the requirements for observing drilling phenomena affecting the penetration mechanism of a PDC bit at a maximum depth of 250 m. The modification mainly includes adding a high power circulation system, high pressure swivel, drilling cell and data acquisition system. Figure 21 shows a schematic view of the setup.

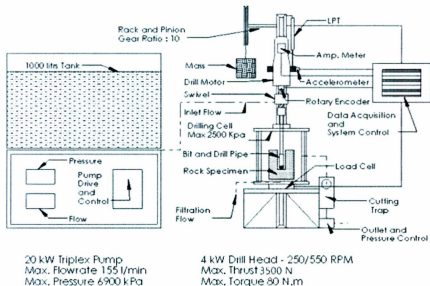


Figure 21. Schematic view of fabricated drill setup

The circulation system pumps water into a rotary drill pipe through a swivel. There is a bit at the end of the drill pipe which can penetrate a rock by applying sufficient load and rotary power. The drilling operations are conducted inside a cell, an environment which is able to handle both the high pressure and high fluid flow conditions of the circulation system. A data acquisition system, including sensors and controllers assists the system to record the data such as pressure, fluid flow, bit load, bit position and power consumption of the drill head, under a safe condition. In addition, pressure gauges are used in several spots of the system. Those gauges assist the driller to manage the operation independently. The fabricated drill setup is presented in Figure 22.

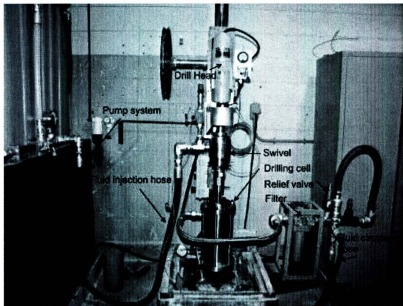


Figure 22. Drill Setup

3.1.1. Rotary System

The rotary system consists of a motor as a rotary head which can provide the maximum bit power of 4 kW. The maximum thrust and torque of this motor are 3500 N and 80 Nm respectively. Figure 23 shows the motor which is attached to a cradle. In addition, the accelerometer and rotary encoder are used for monitoring the vibration of the system and the rotary speed respectively.



Figure 23. Rotary head

3.1.2. Circulation System

The circulation system includes a 20 kW motor installed on a triplex pump which can pump water with a maximum flow rate of 150 L/min and maximum pressure of 6900 kPa. The pump system also includes a variable frequency drive (VFD) to control the flow rate by adjusting the rotary speed of the motor. A water tank, with a capacity of 1000 L, is also located on top of the pump system to supply water as an injection fluid. The circulation system is also equipped with sensors such as flow meter, pressure transducer and water tank level meter to control and record the circulation conditions. Figure 24 shows the pump assembly which is connected to the rig by an injection hose. The other components of the circulation system such as the injection hose, swivel, pressure cell, filter and disposal hose are located on the drill setup.

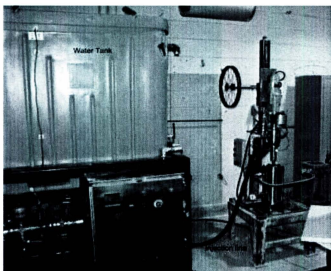


Figure 24. Circulation system

3.1.3. Loading System

A loading system provides the bit with the constant WOB. The weight of the components on the rotary head, which includes the motor, cradle, swivel and drill pipe, is 50 kg. Another source of load is supported by a rack and pinion system with the gear ratio of 10. The loading system is shown in Figure 25. The gear ratio of 10, which is the diameter of the wheel to the diameter of the pinion, causes a static load on bit, which is 10 times greater than the suspended weight.



Figure 25. Loading system

3.1.4. Design of the Swivel

A swivel is required to inject the pumped water into the rotating drill pipe. This swivel which is installed below the drill head (Figure 23) is designed for a flow with a maximum injection pressure of 10,000 kPa. A transparent three dimensional view of the design of the swivel is depicted in Figure 26. The components of the designed swivel are also shown in Figure 27.

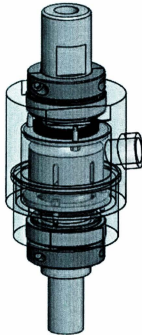


Figure 26. Assembly of swivel

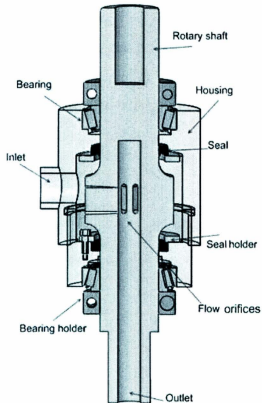


Figure 27. Components of swivel

The inlet of the swivel is connected to an injection housing which comes from the pump outlet. The fluid flow enters the space between the housing and rotary shaft. The shaft is rotating in the center of the housing. High pressure V-lip seals prevent the flow leaking between the rotary shaft and fixed housing. Furthermore, tapered bearings, in

addition to carrying the weight of the housing, keep the rotary shaft centralized in the housing.

3.1.5. Design of the Drilling Cell

In order to build up the BHP during the drilling operation, the rock specimen should be located in an appropriate chamber. Figure 28 shows the transparent view of the designed drilling cell.

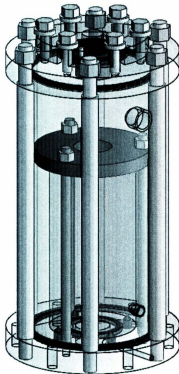


Figure 28. Assembly of drilling cell

The drilling cell is designed for holding a rock specimen with a diameter of 100 mm and a maximum length of 150 mm. The specimen will be clamped in the cell by a plate which is called a specimen holder (Figure 29). There is an O-ring below the rock which separates the center of the rock from applied confining pressure. Through this mechanism it is possible to release any diffused filtrate to atmospheric pressure. In other words, the far field pore pressure becomes zero.

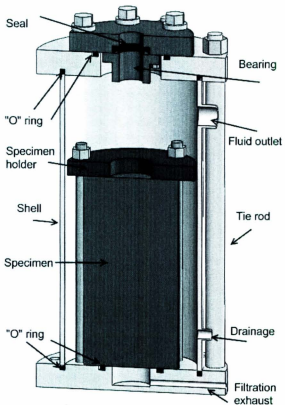


Figure 29. Internal components of drilling cell

Figure 30 shows a drilled rock specimen which is clamped in the bottom cap of the cell. Tie rods are used to assemble the upper cap, bottom cap and shell of the cell. Furthermore, O-rings are used for sealing. The designed pressure of the cell is 2500 kPa with factor of safety of 1.5.

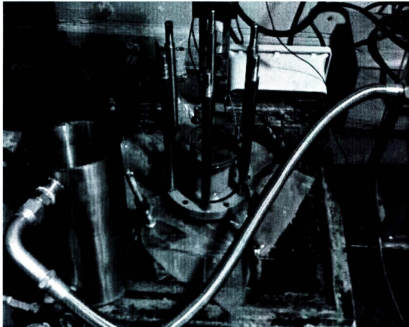


Figure 30. Opened drilling cell with rock specimen

A drill pipe will be passed through the center of the upper cap of the cell. There is a V-lip rotary seal and bearing to seal and centralize the rotating drill pipe in the drilling cell. The outside diameter of the pipe is 24 mm and the inside diameter is 10 mm. A drill bit with a diameter of 35 mm will be attached to the end of the drill pipe. Figure 31 shows

the bit and drill pipe which are passed through the center of the upper cap of the drilling cell.

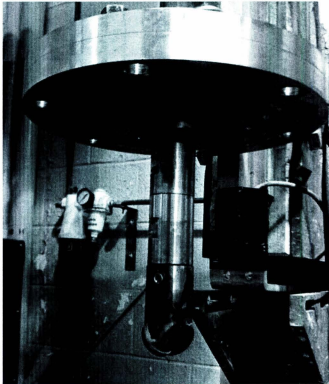


Figure 31. Condition of drill bit in the drilling cell

In order to build up the borehole pressure, an adjustable relief valve is used in the outlet of the drilling cell (Figure 32). The rock fragments and contaminant in the fluid flow will be trapped in a filter prior coming into the relief valve. However, the relief valve is able to pass them.

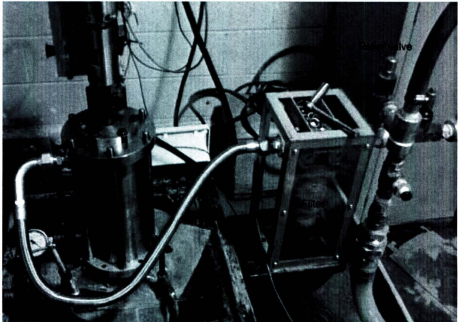


Figure 32. Drilling cell pressure control system

3.1.6. Sensors and Data Acquisition

The drill setup is equipped with sensors to record the drilling parameters during the penetration operation. A load cell is located below the drilling cell to measure the dynamic WOB. This sensor which shows the applied load on the rock provides data with frequency of 512 Hz. In addition, a linear position transducer (LPT) measures the position of the drill head. An accelerometer measures the acceleration of the bit which is oscillating during penetration. An ampere meter is also used to estimate the power consumption of the drill head (for detail see section 5.3.). Pressure transducers measure

the fluid pressure at the inlet of the swivel and outlet of the drilling cell. Furthermore, a flow meter also measures the rate of fluid injection, and a rotary encoder measures the rotary speed of the drill head. All the delivered data are recorded with a sampling rate of 512 Hz on a data acquisition system which is located near the drill setup.

3.1.7. Drill Bit Characteristics

A two cutter micro PDC bit with diameter of 35 mm is used for the drilling experiments. The cutters are brazed to a shank which has the face angle of 25° and back-rake angle of 25° . The cutters also constitute a chamfer with a back-rake angle of 70° . The specifications of the cutter are shown in Figure 33 schematically.

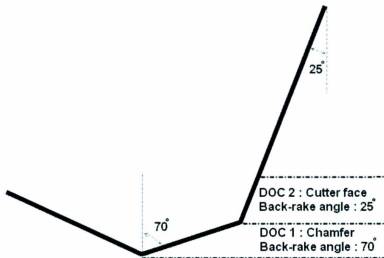


Figure 33. PDC cutter configurations

It can be seen that a cutter has two regions of penetration with respect to the geometry of a rock-bit interface. The first region is the DOC which the chamfer is penetrating, and the second region is the DOC which the face of the cutter is penetrating.

3.1.8. Drill Bit Nozzles Characteristics

The bit requires an additional part to play the role of jet for cleaning the cuttings which will be generated by the PDC cutters. The nozzles are located on the body of the lower part of the bit which is a coupling for attaching the bit to the drill pipe. Figure 34 shows the nozzle configurations. The nozzles are identical with a diameter of 4.445 mm which are inclined 6° outward. The stand off distance of the nozzles to the surface of the rock is 30 mm. For this nozzle configuration the discharge coefficient, C_d , of 0.7 is measured by applying the data of pressure drop and flowrate in Equation (6). This data is obtained from characterizing of the hydraulic system (see Table 1).

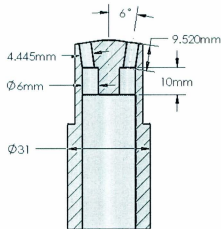


Figure 34. Nozzle configuration

3.2. Drill Setup Characteristics

3.2.1. Jet Flow Characteristics

The drill setup is adapted for appropriate administration of drilling parameters and levels of the test factors. Both the flow rate and ambient pressure of the drilling cell apply an upward force to the drill pipe. The actual WOB of the system should be kept constant. Therefore, in the first step the amount of pump-off force, which is the result of a high velocity water flow and pressure behind the bit nozzles, is estimated. In order to estimate the pump-off force the bit was raised just above the rock surface with distance of less than 1 mm to the rock surface in a drilled hole. This situation is called the off-bottom condition. The pump-off force can be compensated by adding an appropriate mass to the suspended weight to keep the actual WOB at a specific value.

Table 1 shows the pressure behind the nozzle at specified levels of water flow and the resultant pump-off force. Additionally, the other jet parameters, i.e. nozzle pressure drop, jet flow velocity and bit hydraulic power, are reported. The last row of Table 1 also shows the ratio of hydraulic horsepower and the area of bit (HSI) which is commonly used in field drilling operations.

In the next step, the upward force due to pressurizing the drilling cell is estimated. The pressure of the cell is acting on the total area of the drill pipe. The calculation and reading of the load cell are in agreement for an upward hydraulic force of 65 N on the bit under an ambient pressure of 100 kPa. Therefore, an appropriate weight can be added to

the suspended weight, to keep the WOB constant with respect to the condition of the BHP.

Table 1. Jet flow characteristics

Water Flow Rate (L/min)	30	58	86	114	142
Pump-off force (N)	0	45	110	200	320
Nozzle Pressure Drop (kPa)	230	980	2170	3850	5850
Nozzle Velocity (m/s)	16.65	32.2	47.75	63.3	78.8
Bit hydraulic power (kW)	0.11	0.92	3.05	7.17	13.57
Bit HIS (hhp/in.²)	0.1	0.83	2.75	6.47	12.25
Jet Impact Force (N)	50	210	460	820	1260

3.2.2. PDC Bit Characteristics

The coefficient of friction between the PDC cutter and the rock is required for evaluation of the test results. This value is estimated through a simple test under a low WOB of 100 N, in which the bit does not penetrate the rock. In this load on bit condition a battery is used to rotate the motor. The voltage of 5.46 V and current of 3.28 A is recorded which give the power consumption of 17.9 W. The power consumption is also attained when the bit is adjusted in the off-bottom position. The voltage of 5.8 V and current of 1.2 A is recorded which give the power consumption of 6.95 W. The difference between the motor power consumption in these two conditions is multiplied by the considered efficiency of the motor which is 80%. Therefore, the pure power consumption of motor which is only used for overcoming the friction between the PDC cutters and rock surface

is approximately 8.76 W. Multiplying the pure power consumption of 8.76 W to the rotary speed of 0.5 gives the torque on bit of 4.375 N.m. Consequently, for the bit with radius of 17.5 mm under the load of 100 N, the coefficient of friction between PDC cutter and rock, (μ_0), will be 0.25. Equation (10), (11) and (12) show that how the coefficient of friction is calculated from reading of the power consumption of the drill head in the on-bottom and off-bottom conditions.

$$\text{Pure Power consumption} = \text{Motor Efficiency} \times (\text{Power consumption}_{\text{on bottom}} - \text{Power consumption}_{\text{off bottom}}) \quad (10)$$

$$\text{Torque} = \text{Pure power consumption} \times \text{Bit revolution per second} \quad (11)$$

$$\mu_0 = \frac{\text{Torque}}{\text{Bit Radius} \times \text{WOB}_{(\text{no penetration})}} \quad (12)$$

4. Preparation and Characteristics of rock specimen

4.1. Study of Grain Size Distribution

In order to prepare a rock sample for drilling tests, concrete slurry is molded in cylinders with a diameter of 100 mm. The concrete slurry includes aggregates, cement and water.

The size distribution of the aggregate is studied using eight sieves. Table 2 shows the relation between the mesh number of the sieves and range of grain sizes. The last column of Table 2 is the label of each range of the sizes.

Table 2. Result of grain size analysis

Sieve No.	Size range	Passes weight %	Label
4	Above 4.75 mm	3.81	1
8	4.75-2.365 mm	4.9	2
10	2.365-2 mm	12.98	3
16	2-1.2 mm	26.76	4
20	1.2-0.5 mm	10.27	5
40	0.5-0.42 mm	15.46	6
60	0.42-0.25 mm	3.46	7
100	0.25-0.15 mm	20.93	8
-	Below 0.15 mm	1.44	9

The grain distribution is presented in Figure 35, in which the points show the passing weight percentage from above indicated sieves (Table 2).

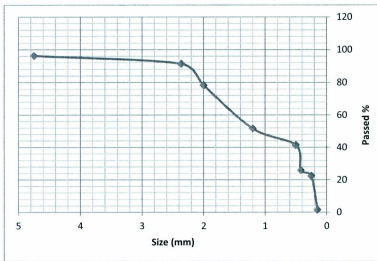


Figure 35. Grain size distribution of aggregates used in rock specimen

Figure 36 also presents the sieved aggregates, regarding aforementioned labels. Figure 36 shows that the aggregate with a size of greater than 4.75 mm, in comparison to the other sizes, constitutes a low mass percentage. These big aggregates may cause a significant irregularity in the matrix of the specimen, and yield large errors in the unity drilling responses. Therefore, these aggregates have been removed from the bulk of material. The rest of the sand is mixed with cement and water to prepare the concrete slurry. The cement-aggregate mass ratio is 33%, and the water-cement mass ratio is 40%.

A vibratory rod is also used to minimize void spaces in the concrete matrix. The samples are cured for 120 days in water at a temperature of 25°C.

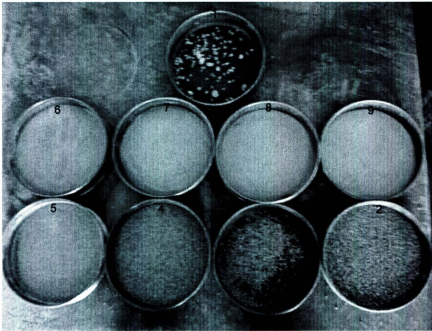


Figure 36. Sieved aggregates are labeled as indicated in table 2.

4.2. Physical Properties of the rock specimen

The physical properties of the rock are evaluated on core plugs with a diameter of 46 mm, which are produced from the center of the prepared rock specimen using a diamond coring bit. The elastic moduli and strength of the intact specimen is measured based on the ASTM standard D7012-10 [47]. Table 3 shows properties of the rock specimens.

Figure 37 shows the shear plane of a core plug, which is retrieved from the specimen, after failure in a UCS test. Figure 38 also shows the surface of the rock after

surface grinding. The surface represents the distribution of the aggregates in the matrix of the specimen.

Table 3. Physical properties of the rock specimen

UCS	52 MPa
Tensile Strength	5.4 MPa
Young's Modulus	29 GPa
Poisson Ratio	0.15
Effective Porosity	29%
Internal Friction Angle	40°

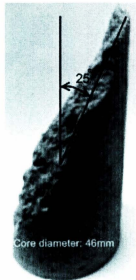


Figure 37. Shear plane in a core plug after UCS test

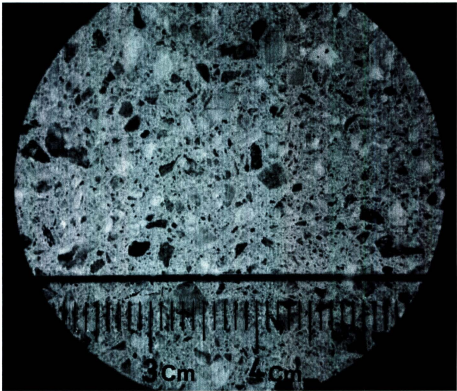


Figure 38. Surface of the rock specimen after surface grinding

The rock samples are coated with an impermeable adhesive material, which prevents the radial invasion of water into the rock specimen prior to tests and during penetration.

5. Design of Experiment

5.1. Design of Experimental Test Matrix

Based on the performed literature review and achievements of previous investigations, the BHP and BHC are considered the main influential factors in the performance of a drill bit at great depth. Increasing the pressure of the drilling cell provides BHP or hydrostatic pressure of the mud column on the surface of rock in deep well drilling operations. In addition, the circulation system, with respect to the design of the nozzle, is able to provide a hydraulic power greater than three times the mechanical power of the bit. This great value of bit hydraulic power is sufficient to investigate the effect of the jet further than previous investigations have performed.

The BHP varies over three levels of 130, 1100 and 2100 kPa (gauge pressure), which is proportional to drilling operations at depths of 13, 110 and 210 meters. The level of the flow rate mainly varies over four levels of 30, 58, 86, 114 L/min.

A constant WOB of 1600 N has been applied on the bit for the entire test. However, the amount of the recorded pump-off force and hydraulic force are also added to the WOB to keep the WOB constant at different applied conditions of BHC and BHP.

A full factorial test with four replications is performed on the main 12 points of the experiment, which are four tests at the specified levels of flow rate for each three levels of BHP. Additionally, complementary tests are performed for further clarification of the hypothesis. Several tests are performed at the flow rate of 142 L/min under higher BHP. The circulation system in this condition supports the bit with a hydraulic power of 13.5

kW. Moreover, complementary tests with no use of circulation and use of air as drilling fluid are conducted.

ROP, MSE and inlet pressure of the bit, at each specified level of BHP and flow rate, are evaluated as the main results of the experiment.

5.2. Experimental Test Procedure

A test procedure is defined for maximizing the quality of the drilling responses. After the installation of the rock samples, the desired flow rate, regarding the test matrix, is applied. The relief valve is also adjusted so that the ambient pressure of the drilling cell becomes equal to the desired value.

The rock specimen is predrilled for 15 mm, in which all the face of the bit meets the rock surface. Before starting the rock penetration the rotary head is kept off-bottom, and both the circulation system and drill head are turned on. The data acquisition system is adjusted to the recording mode and the information of the power consumption is recorded. This is because, at each level of the tests, the motor power consumption is altering by different frictional forces of the seals, due to different pressure conditions in swivel.

Drilling operations are started after 5 seconds of rotation of the bit in an off-bottom condition.

5.3. Experimental Data Analysis

Power consumption of the motor is estimated by multiplying the recorded data of ampere meter by the voltage which is assumed to be 115 V. The motor efficiency of 80% is

considered for calculation of the delivered mechanical power to the bit. The power consumption of the bit is estimated by subtracting the power consumption of the motor during penetration from the power consumption of the motor before penetration. The torsional MSE of the tests is estimated by dividing the bit specific power by ROP as was shown in the section 2.1 (Equation (2)). In the calculation of total MSE, the resultant stress from the source of WOB, which is 1.63 MPa, is added to the torsional MSE. This stress is calculated by dividing WOB by the area of the bit. Equation (13) shows the calculation of total MSE.

$$\text{Total MSE} = \frac{\text{Power consumption of drillhead}}{\text{Drill bit area} \times \text{ROP}} + \frac{\text{WOB}}{\text{Drill bit area}} \quad (13)$$

ROP of the tests is also estimated by calculating the slope of the curve of bit position vs. time. Data of the bit position is provided by the LPT. The evaluation of the recorded data is performed on the collected drilling responses after 5 seconds of the drilling operation. This lapse time is required for evaluating the bit performance in a steady state condition.

5.4. Design of Simulation Test Matrix

The main purpose of the DEM simulation is investigation of drilling phenomena with more focus on the influence of vibrations of the cutter on penetration mechanism. In addition, the DEM simulation studies the drilling parameters which are not investigated in the experimental test. Therefore, study of the effect of WOB, rotary speed and inertia of

the drill bit on the penetration mechanism of PDC bit is conducted in a simulated environment. In this numerical simulation, the aforementioned parameters are tested on a single cutter which penetrates a rock block linearly. Therefore, the expressions of WOB, rotary speed and inertia of the bit are changed to load on cutter, horizontal speed of cutter and mass of the cutter, respectively.

All the simulation test factors are studied over three levels in a full factorial test. In addition, no replication is conducted, as the simulation gives similar results with replication. The BHP and BHC, which in the simulation test are called rock confining pressure and cutter cleaning, are considered as the fixed test parameters. The response of the horizontal penetration is DOC and MSE.

6. Results, Discussion and Analysis of Experiments

6.1. Results of Experiment

The results of the tests are in terms of the ROP and MSE. Figure 39 shows the average ROP of four replications vs. flow rate for selected levels of BHP. The error bars show the full range of experimental data. The BHP imposes a negative effect on ROP, and the bottom-hole cleaning imposes a positive effect on ROP. However, there are optimum points for the flow rate which are dependent on the condition of BHP. The optimum point of the flow rate for the lowest BHP is 60 L/min (HSI = 0.83) and for higher BHPs is 114 L/min (HSI = 6.47).

The curves of ROP vs. flow rate (Figure 39) indicate that the amount of reduction in ROP, when BHP is varied from 130 KPa to 1100 KPa, is higher than the amount of reduction in ROP, when BHP is increased from 1100 KPa to 2100 kPa.

Figure 40 shows the average MSE vs. flow rate for selected levels of the BHP. The MSE is varying in an inverse trend of ROP with respect to change in the conditions of the BHP and bottom-hole cleaning.

The minimum recorded MSE is approximately 164 MPa. The high value of MSE, in comparison to the recorded UCS of the rock specimen which is 52 MPa, implies that, the applied conditions of the drilling test results in a maximum drilling efficiency of 32%, which is calculated by dividing MSE to UCS of the rock. The conditions of the test, such as applied WOB, bit geometry and use of strong aggregates (granite and feldspar) in rock

preparation are assumed to be the main reasons for the highest achieved drilling efficiency.

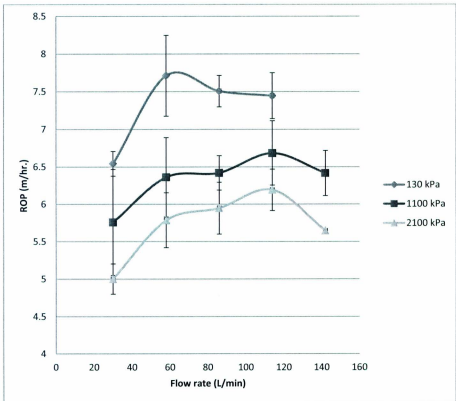


Figure 39. ROP vs. flow rate and BHP

The results of the tests illustrate that the minimum MSE at higher BHP can be achieved at greater levels of flow rate. However, further increase in the flow rate increases the amount of MSE. In general, an increase in MSE at flow rates higher than the optimum levels implies that the bit faces a harder condition of penetration.

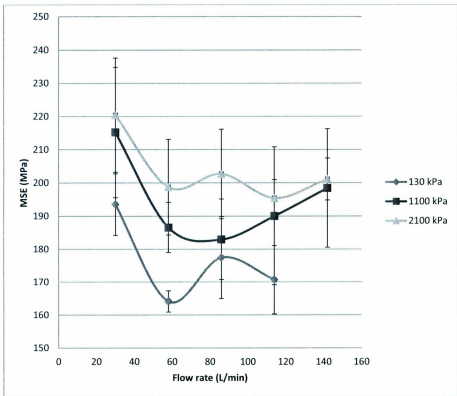


Figure 40. MSE vs. flow rate and BHP

The optimum level of the flow rate for MSE of the penetration, under BHP of 130 kPa and 2100 kPa, is in agreement with the optimum hydraulic condition for ROP. However, there is a marginal disagreement between minimum MSE and maximum ROP under BHP of 1100 kPa.

A single experiment has been performed under atmospheric conditions and without water flow. The MSE of the test at the early period of the penetration, 5-10 seconds, was

measured as 195 MPa with DOC of 0.182. Additionally, it has been observed that the bit performance becomes worse with continuation of penetration under the no circulation condition. For the next period of time, 10-15 seconds, the MSE is measured as 250 MPa with the average DOC of 0.174 mm. Further continuation of the drilling yields ROP of near zero. The bit floundering in previous crushed material is one reason for the high value of MSE and low value of ROP. Figure 41 shows a balled up bit after performing only 20 mm rock penetration.



Figure 41. Balled up PDC bit

In one experiment, air flow is used as the drilling fluid with a back pressure of 70 kPa behind the nozzles. This condition of drilling results the bit floundering due to a low hydraulic power. The MSE of the penetration is measured as 240 MPa with an average DOC of 0.19 mm. The high value of MSE can be related to the higher frictional energy losses in a dried rock-bit interaction.

The PDC bit has axial vibrations in all the drilling tests. The axial vibration causes fluctuations in the readings of the load cell. The load fluctuations are random and irregular in both magnitudes and frequencies. However, the RMS of the load fluctuations is measured at 200 N for the entire tests.

6.1.1. Effect of Flow Rate on Drilling Responses

The PDC cutters have a chamfer with back-rake angle of 70° at a vertical depth of 0.15 mm (Figure 33). The calculated DOC from the results of ROP shows that the main part of penetration, regarding the applied WOB, is performed in front of the chamfer. Therefore, the face of the cutter which constitutes back-rake angle of 25° is less involved with the penetration operation. In addition to ROP, DOC is also used as a test result to study the influence of test factors with respect to the geometry of the rock-bit interface. DOC is calculated by dividing the ROP by twice of rotary speed (250 rev/min), as there are two identical PDC cutters on the bit.

Table 4 shows the results of the tests in term of average DOC with respect to the jet parameters and BHP.

Table 4. DOC vs. BHP and jet parameters

BHP (kPa)	Flow rate (L/min)	Jet velocity (m/sec)	Jet impact force (N)	HSI (bhp/in²)	DOC (mm)
130	30	16.65	50	0.1	0.211
	58	32.2	210	0.83	0.249
	86	47.75	460	2.75	0.242
	114	63.3	820	6.47	0.240
1100	30	16.65	50	0.1	0.186
	58	32.2	210	0.83	0.205
	86	47.75	460	2.75	0.207
	114	63.3	820	6.47	0.216
2100	30	16.65	50	0.1	0.162
	58	32.2	210	0.83	0.187
	86	47.75	460	2.75	0.192
	114	63.3	820	6.47	0.200
1100	142	78.8	1260	12.25	0.207
2100	142	78.8	1260	12.25	0.182

Figure 42 shows the result of DOC vs. jet velocity (U_n) for the three specified levels of BHP. The jet velocity is calculated by dividing the flow rate to the total flow area (TFA) of the nozzle.

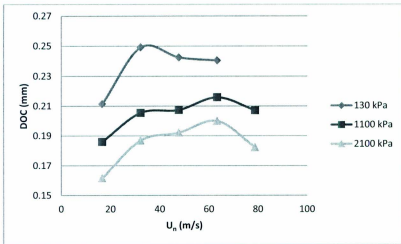


Figure 42. DOC vs. flow rate

Figure 43 also shows the result of DOC vs. jet impact force at specified levels of BHP.

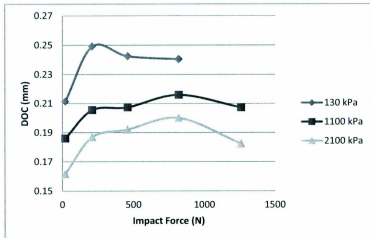


Figure 43. DOC vs. jet impact force

Figure 44, which shows the result of DOC vs. HSI at specified levels of BHP, shows the same trend with the curve of DOC vs. impact force.

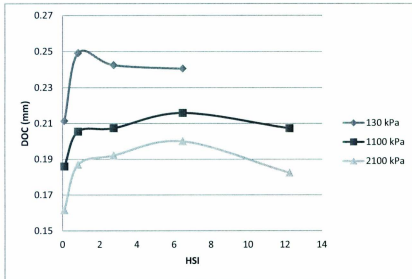


Figure 44. DOC vs. HSI

From all the figures the existence of an optimized condition of jet parameters can be observed. In addition, increasing BHP, from 130 kPa to 1100 kPa, causes the optimum level of flow rate shifts to larger value. These results imply that the effect of the BHP and BHC should be investigated simultaneously.

It has also been observed that the fluid flow contributes to penetration by cleaning the generated particles. Figures 45 and 46 shows the differences in the zone of the penetration between drilling of similar rock samples under the same BHP of 1100 kPa

with two different bottom hole cleaning conditions, which are flow rates of 30 L/min and 114 L/min. The pictures are taken after raising the bit from the rock surface. It can be seen that the only difference between these two conditions of drilling is removing the crushed material which can accumulate between the PDC cutter and rock.

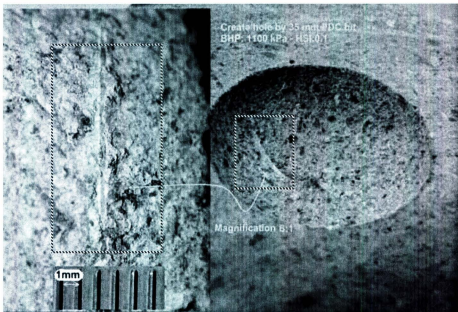


Figure 45. Accumulation of crushed material between rock and cutter

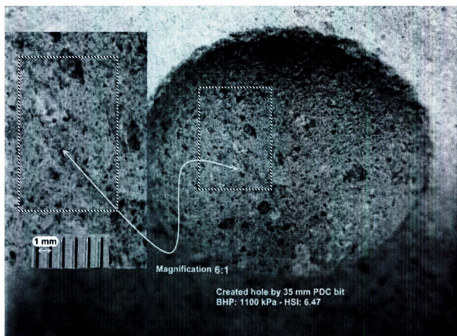


Figure 46. Cleaned rock-cutter interface at high jet flow condition

6.1.2. Effect of BHP on Drilling Response

The negative effect of the BHP on bit performance, which is reduction in ROP and increase in MSE, can be clearly seen in the tests. In order to explain the influence of the BHP, the rock failure in front of a PDC cutter is compared to a rock failure in a simple compressive strength test. Figure 47 schematically shows the rock failure under the principal stress of " σ_1 " with confining pressure of " σ_3 " with the related Mohr-Coulomb failure criteria. The value of the σ_1 , when there is no confining pressure, is the unconfined compressive strength (UCS). The angle between the failure shear plane and the major stress is called the shear plane angle (θ). This value can be used for calculation of the

rocks' internal friction angle (Φ) which is used in Mohr-Coulomb failure criteria. This relation is shown in Equation (10).

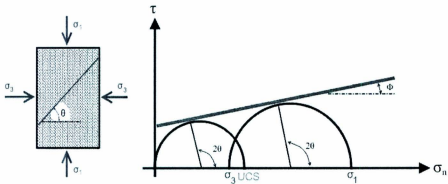


Figure 47. Rock failure in a compressive strength test and Mohr-Coulomb failure criteria

$$\Phi = 2\theta - 90 \quad (14)$$

In case of the existence of confining pressure (σ_3) the value of principal stress (σ_1), which yields rock failure, will be shifted toward greater values with respect to the rocks' internal friction angle (Figure 47).

In a drilling operation of a PDC cutter, the major stress is provided by both horizontal and vertical forces of the cutter, and any pressure on the rock surface, e.g. BHP, is acting as a confining pressure. The rock failure under a vertical load can occur similar to the penetration mechanism of a roller cone bit, especially because the PDC

cutter has axial vibrations. In order to study the effect of the BHP on the penetration mechanism of the PDC cutter, the results of the test for MSE are useful. The MSE of a test represents the strength of the rock with which the drill bit faces during rock penetration.

In order to estimate MSE under a specific BHP, the following assumptions have been considered. First, the Mohr-Coulomb failure envelope is linear. Second, the rock internal friction angle is 40°. Third, the minimum recorded MSE (164 MPa) can be used as a basis for the rocks' apparent strength in the evaluation of all the other drilling tests. The base MSE is a value which is achieved under the influence of all known and unknown drilling parameters. Therefore, it can be assumed that any increase in the value of MSE is related to the test variables.

Using aforementioned assumptions and based on the relations between the principal stress (σ_1) and confining stress (σ_3) in Mohr-Coulomb failure criteria, a correlation between these stresses has been extracted, which is shown in Equation (11). The units are in MPa.

$$\sigma_1 = \frac{1 + \sin\Phi}{1 - \sin\Phi} \times \sigma_3 + (\text{Minimum MSE}) \quad (15)$$

Or

$$\text{MSE} = 4.6 \times \text{Confining Pressure} + 164 \quad (16)$$

The above indicated correlation implies that for a rock with the internal friction angle of 40° , when the confining pressure is increased by 1100 kPa, the value of the σ_1 , which the bit faces with, or MSE will be increased by only 5 MPa.

The results of MSE illustrates that at a flow rate of 30 L/min, an increase in BHP from 130 kPa to 1100 kPa increased the MSE approximately 21.7 MPa, which is much greater than the expected value of 4.6 MPa. However, at this level of cleaning, further increase in BHP from 1100 kPa to 2100 kPa raised the MSE 5.2 MPa, which is close to the expected increase of 4.6 MPa.

This observation implies that the BHP may not be the only parameter which increases the rocks' apparent strength, and there are other effective parameters which are dependent on the BHP.

Figure 48 shows that an increase in flow rate divides the curve of ROP into two regions. The first region is where the increase in hydraulic power increases the ROP, and the second zone is where the increase in the flow rate decreases the ROP. The second region, where the ROP is decreased, can be observed at a lower flow rate for the lower BHP. Therefore, an optimal condition can be observed for bit hydraulic power.

The existence of an optimal condition in the curve of ROP vs. the flow rate implies that higher hydraulic power is not always accompanied by a higher ROP. In the other words, increase in the power of the bit hydraulics can improve the ROP up to a specific point and further increase in the hydraulic power may reduce the bit performance.

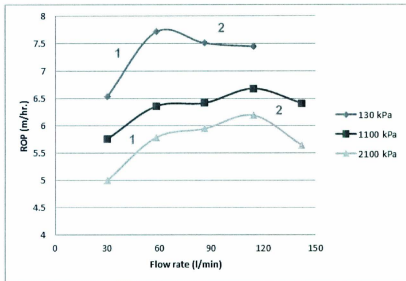


Figure 48. Ascending zone and descending zone in the curve of ROP vs. flow rate

Figure 49 is schematic of a PDC cutter-rock interaction under low BHP. The cuttings in front of the cutter after failure are easily ejected from the rock-bit interface, especially if the back-rake angle of the cutter (β) is smaller than the angle of the shear plane (θ) in front of the cutter. In this condition there is a wider space for the generated fragments to be removed from the zone of the penetration (Figure 49). On the other hand, in the chamfer of the cutter, the rock failure can be more affected by the containment of cuttings under a higher back-rake angle.

Figure 50, which shows the rock after the drilling test under the BHP of 130 MPa with the flow rate of 30 L/min, confirms the existence of crushed material beneath the chamfer.

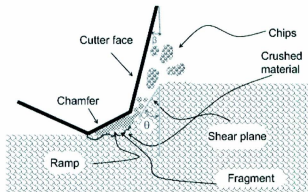


Figure 49. Penetration under low BHP

Both the low ROP and high MSE for this condition of the test can be related to poor BHC. Therefore, in a low BHP condition, although the surface fragments are cleaned easily, it is still necessary to spend hydraulic power on cleaning the powdered cuttings in front of the chamfer, as the crushed rock fragments, due to a specific orientation of the rock-bit interface, tend to remain in this zone. It is speculated that by an appropriate cleaning of this part, both the MSE and ROP will reach an optimum point.

Additionally, Figure 51 shows the cuttings which are trapped in the filter of the circulation system. The cuttings are collected from the drilling test under BHP of 2100 MPa with a flow rate of 86 L/min. These fragments have approximate diameter of 0.1 mm to 1mm. However, larger fragments might be undrilled aggregates which are pulled out of the matrix of the specimen due to the failure of the cemented bonds.

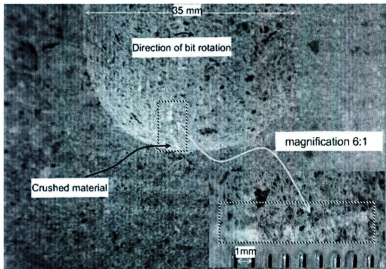


Figure 50. Accumulation of crushed material under low BHP and poor BHC



Figure 51. Collected cutting from filter under BHP of 2100 kPa and flow rate of 86 L/min

Figure 52 schematically shows a PDC cutter-bit interaction under higher BHP. BHP (P_c), which acts as a confining pressure, in addition to the role of rock strengthening, holds the crushed cuttings in the zone of the generation.

One of the reasons of the hold-down is that the pressure in the shear plane due to dilatation is very low. Moreover, diffusion of the borehole fluid in this zone, due to a very low permeability, is slow. Therefore, the main part of the BHP acts as a holding force on the fragments. Moreover, the generated fragments in front of the chamfer, in case of insufficient bottom-hole cleaning, can be crushed beneath the chamfer of the cutter to fine particles. Therefore, under higher BHP, a higher cleaning power is required to eliminate the effect of the hold-down force. This is why the optimum points in the curve of ROP and MSE vs. flow rate, under the higher BHP, are shifted toward higher flow rates.

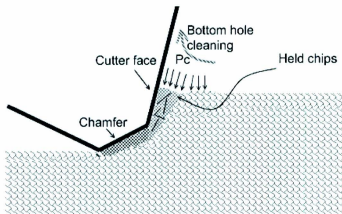


Figure 52. Rock-cutter interaction under elevated BHP

The negative effect of the BHP, in addition to the rock strengthening, is shown to be hold-down of the cuttings. The generated cuttings under hold down force are being crushed before exiting from the rock-cutter interface. The experimental results show that lower values of ROP and higher values of MSE are accompanied by the existence of a zone of crushed material under the chamfer of the cutters.

6.2. Mechanism of BHP in rock confinement

It has been argued that the observed MSE of the penetration poses a lack of fit with the applied BHP. In addition, it has been shown that containment of fine cuttings can be a strong hypothesis for the increase in MSE and a reduction in the value of ROP. The crushed materials in the test under BHP of 130 kPa with a flow rate of 30 L/min, due to low BHC, results in MSE of 193 MPa, which is considerably higher than the minimum MSE value of 164 MPa. Additionally, increasing the BHP to 1100 kPa yields the MSE of 215 MPa under the lowest level of flow rate. Based on the achieved correlation (Equation 12), the MSE of 215 MPa, in comparison to the MSE of 164 MPa, calls for a value of confining pressure of approximately 11,000 kPa on top of the region where the fragment is generated. However, the BHP has been raised only 1000 kPa. Therefore, there is another source, i.e. containment of cutting flow, which applies an additional 10,000 kPa confinement on the zone of penetration and result in an unexpected increase in MSE of approximately 46 MPa.

Moreover, a small increase in MSE by raising the BHP from 1100 kPa to 2100 kPa, at the lowest level of the flow rate, indicates that no further containment of fragments can occur. In other words, for the low level of cleaning, increase in borehole pressure to 1100

kPa causes the most of the generated cuttings to stay beneath the cutter. Therefore, in such a condition, further increase in BHP causes an expected growth in the value of MSE with respect to the Equation 12.

In order to discover the mechanism of a great rock confinement under the influence of crushed materials, a schematic model of rock-bit interaction, regarding the defined parameter of the drilling test, is depicted in Figure 53. In a drilling operation, a vertical load is applied on the bit, and the bit is being rotated. The horizontal force is the result of rotation and subsequent rock-bit interactions.

It has also been shown that the accumulation of the generated fragments can be more significant, under confinement of the BHP (P_c) and lower fluid flow removal pressure (P_s). It is clear that the cratering under the tip of the cutter can be more efficient when a higher horizontal stress and vertical stress are directly applied on the rock surface. The generated rock fragments under the force components of the cutter can be crushed to fine particles in the case of a shortage in cleaning. One of the sources of the rock confinement can be the flow of the cuttings underneath the cutter (P_{cf}).

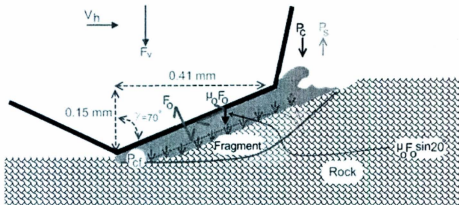


Figure 53. Flow of crushed cuttings in rock-cutter interaction

In order to simplify the rock-bit interaction, it has been assumed that a cutter, with the length of 35 mm (diameter of the bit) and similar described configuration of the cutters of the bit, is penetrating a rock under a vertical load (F_v) by applying a horizontal speed (V_h). The results of drilling tests for DOC indicate that the main part of penetration is conducted in front of the chamfer with back-rake angle of 70° . Additionally, in such a condition, the fragments can be crushed and protrude out of the rock-cutter interface due to compression.

The coefficient of friction between the particles of the rock specimen is estimated to be 0.84 based on the rock internal friction angle of 40° . Furthermore, the coefficient of friction between the PDC cutters and rock (μ_o) has been found to be 0.25. The lower coefficient of friction between the PDC cutter and crushed rock implies that the fragments and crushed material, in the case of compression and containment, tend to slide on the face of the bit with the advancement of the cutter. However, the sliding of cuttings on the

cutter face can also be related to the inclination of the shear plane and back-rake angle, because, the value of friction in addition to the coefficient of friction is dependent on the value of the normal force which causes friction. A normal force can be applied less on the fragments with greater values of the shear plane angle. In this case study, experimental observations show that the shear plane under the chamfer is parallel with the face of the chamfer.

An analysis of the rock-bit interaction is performed to estimate the amount of rock confinement due to the flow of cuttings under the cutter. The following assumptions are also considered in this analysis. First, a fixed load, which is equal to WOB, is acting on the bit. Second, due to smooth axial vibrations of the bit, there is no contact between the tip of the cutter and the rock surface. Equation (13) shows the force equilibrium in the direction of applied load on the cutter (F_v).

$$F_v - F_0 \times \mu_a \times \cos \gamma - F_0 \times \sin \gamma = 0 \quad (17)$$

Therefore, the value of the “ F_0 ” can be determined by Equation (14).

$$F_0 = \frac{F_v}{\mu_0 \cos \gamma + \sin \gamma} \quad (18)$$

The vertical component of the existing frictional force exerts a confining pressure on the rock-cutter interface. This pressure can be calculated using Equation (15).

$$P_{cf} = \frac{F_v \times \mu_o}{\mu_o \cos \gamma + \sin \gamma} \times \frac{\cos \gamma}{A_o} \quad (19)$$

where, “A_o” is the horizontal area under the chamfer which is given below.

$$A_o = 35 \times \text{DOC} \times \tan \gamma \quad (20)$$

The resultant vertical component of the frictional force is acting on this area. The value of the horizontal area is estimated by multiplying the horizontal length of the chamfer (0.41mm) by the length of the cutter which is considered equal to the diameter of the bit (35 mm). In the estimation of “A_o” it is assumed that no accumulation of the cutting exists in front of the cutter face which has a back-rake angle of 25°, as is shown in Figure 53.

Applying other conditions of the penetration, which are WOB of 1600 N, a friction coefficient of 0.25 and back-rake angle of the chamfer (γ) of 70°, in Equations (15) and (16) yields a cutting flow pressure (P_{cf}) of 9000 kPa. The calculated confining pressure, despite administered simplifications and assumptions, is very close to the unexpected confining pressure of 10000 kPa which was theoretically suggested.

BHP not only yields accumulation of the cutting material, but also applies a downward force profile on the cuttings which can be added to the value of the friction. However, calculation of this force is related to a complicated pressure profile inside the cuttings and the surface area where the pressure is acting.

In the performed set of experiments, based on the measured value of DOC, the cutters penetrate the rock mainly under their chamfer. In the test with a flow rate of 30 L/min, when the BHP was increased from 1100 kPa to 2100 kPa, despite a significant reduction in the value of DOC, the value of MSE increased with respect to the expected rock strengthening. Since, for the higher BHP condition, the value of DOC is still higher than vertical length of the chamfer, the confinement is still happening under all of the horizontal area of the chamfer (35mm×0.41 mm). Therefore, the confinement of cutting flow can be similar for the BHP of 1100 kPa and 2100 kPa, at the lowest level of BHC. Also, a cleaned region in front of the cutter face, under HSI of 0.1, results in a small difference between the MSE of the tests under BHP of 1100 kPa and 2100 kPa. The aforementioned phenomena were also reported by Maurer [10], who showed that when a single tooth acts on a rock surface, an increase in borehole pressure by water results in no significant changes in the load of penetration and reduction volume of a crater.

The restriction of the bit performance is not only related to the flow of crushed material. Other parameters, such as friction in the tip of the cutter and confinement of the penetration zone by the applied WOB with the specific back-rake angle of the cutter, also decrease drilling efficiency. However, the aforementioned negative effects are considered to be approximately the same for the entire test.

It should be also considered that, despite applying a low level of flow rate of 30 L/min, the cuttings are being cleared and transferred out of the borehole. A complete stopping of cleaning can result in bit balling. Such a condition of drilling, even in

atmospheric conditions, can result in a higher MSE than a pressurized condition with the lowest level of the applied BHC.

It has been shown that the difficulties in rock penetration, in addition to the high BHP and low bottom-hole scavenging, are a function of the friction and back-rake angle of the cutter. Therefore, reduction in friction between the face of the cutter and the cutting material, reduction of the back-rake angle, and cleaning of the generated cuttings can improve the penetration performance of a PDC bit in the presence of a high BHP.

6.3. Mechanisms of jet flow in bottom hole cleaning

The main effect of the fluid flow in the penetration mechanism of a PDC bit is shown to be the cleaning of cuttings which are generated by the cutters. The source of hydraulic removal force, under the action of a high velocity jet flow, is the drag force on the cuttings which according to Rayleigh's equation is related to the square of the velocity of a flow stream acting on a specific area of cuttings.

On the other hand, the change in a fluid flow velocity in a region yields a change in the pressure on that zone. Bernoulli's principle implies that an increase in fluid flow velocity is accompanied by a reduction in pressure. Equation (17) shows Bernoulli's principle.

$$\frac{U^2}{2} + gZ + \frac{P}{\rho} = \text{Constant} \quad (21)$$

where “U” is the fluid flow velocity, “g” is the acceleration due to gravity, “Z” is the elevation of the point above a reference plane, “P” is the pressure at the selected point, and “ ρ ” is the density of the fluid.

The experimental data shows that the BHP can be locally altered by a change in the jet flow velocity. Table 5 presents the nozzle back pressure (P_n) under the adjusted BHP (P_c) with respect to the fluid flow velocity (U_n) in the nozzle. It can be seen that at higher BHP, the nozzle pressure drop is less than the sum of the adjusted BHP (ambient pressure) and recorded pressure drop of the nozzle when the exhaust is open to atmospheric pressure (P_o). This means that the pressure, ahead of the nozzle and in the space above the rock surface, due to a high velocity of water flow, has been reduced to a value below the adjusted BHP. This reduction, which is shown in the last column (P_r) of the Table 5, is calculated by subtracting the expected nozzle inlet pressure ($P_o + \text{BHP}$) from the real recorded nozzle inlet pressure (P_n). The value of “ P_r ” is calculated for all levels of the jet flow velocity (U_n) under BHP of 1100 kPa and 2100 kPa. Figure 54 shows the curve of reduced pressure vs. flow velocity in the nozzle. Deflection of the curve at a BHP of 1100 kPa illustrates that the jet velocity of 65 m/s is sufficient to reduce the BHP of 1100 kPa to a value less than atmospheric pressure. In such a low pressure condition water cavitation occurs and results in reduction of ambient pressure. The resultant pressure pulse of the cavitation may improve the bottom hole cleaning.

Table 5. Pressure drop in the nozzle

P_c (kPa)	U_n (m/s)	P_o (kPa)	P_n (kPa)	P_r (kPa)
1100	16.12	230	1210	120
	31.16	980	1725	355
	46.21	2170	2620	650
	61.25	3850	3930	1020
	76.29	5850	5860	1090
2100	16.12	230	2200	130
	31.16	980	2725	355
	46.21	2170	3620	650
	61.25	3850	4830	1120
	76.29	5850	6205	1745

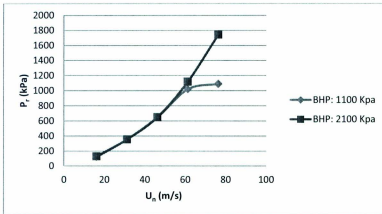


Figure 54. Reduced pressure ahead of nozzle vs. nozzle velocity

The amount of reduced pressure (P_r) is plotted vs. square of the jet velocity (U_n^2) in Figure 55. It can be seen that there is a linear relationship between the above indicated parameters.

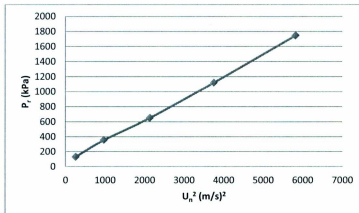


Figure 55. Reduce pressure ahead of nozzle vs. square of nozzle velocity

Equation (18) shows the correlation between reductions in pressure ahead of the nozzle vs. jet velocity in SI units.

$$P_r = 288 \times U_n^2 - 54 \quad (22)$$

Therefore, it can be asserted that a jet stream, due to a high velocity flow, creates a low pressure region above the surface of the rock. However, when the flow streams arrive at the rock surface, the direction of the flow will be changed. Consequently, the velocity on the surface instantaneously reaches zero. Therefore, the rock surface constitutes a high pressure and the space above the surface constitutes a low pressure. The surface pressure is radially distributed which becomes smaller at farther radial distance. The imposed surface pressure may intensify the chip-hold down phenomenon.

Figure 56 depicts the aforementioned condition in a three dimensional view. The region which is indicated by 1 is the low pressure zone, due to high velocity of fluid flow. Region 2 in the rock surface, which is close to the jet exhaust, has a high pressure, and the surface pressure distributes radially and becomes lower in zones 3 and 4. The surface pressure can cover part of the rock surface in front of the cutter, where the cuttings are being generated.

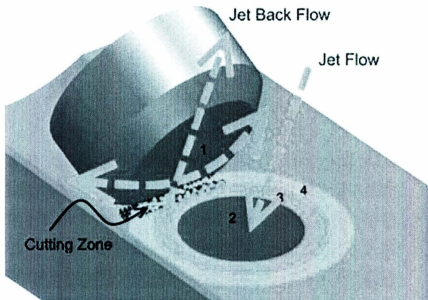


Figure 56. BHC in front of PDC cutter

Figure 57 shows the zone of the penetration, with 20 times magnification, after raising the bit, from the rock surface which has been drilled under the BHP of 2100 kPa and flow rate of 142 L/min. Despite applying a very high flow rate, an accumulation of cutting material can be seen.

Reduction in performance of the bit, by applying a very high jet flow, is observed for all the levels of BHP. In addition, under an elevated borehole pressure condition, despite implying an optimum flow condition, the value of MSE is still higher than the value which is expected to be observed with a small increase in BHP.

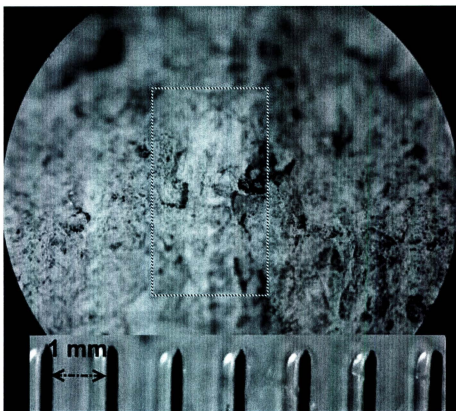


Figure 57. Accumulation of powdered cuttings in the zone of penetration for the test under BHP of 1100 kPa with flow rate of 142 L/min

Furthermore, even though all the nozzle back pressure causes rock strengthening, the amount of observed MSE is still higher than the value which is expected to be observed. Moreover, small difference in MSE value for the test under BHP of 1100 kPa and 2100 kPa with flow rate of 142 L/min (Figure 40) implies the dominant role of the jet flow in the confinement of the rock surface.

Based on the aforementioned observation, it can be asserted that the applied surface pressure may play the role of hold-down pressure for the cuttings which are being generated under the cleaned condition. In a great surface pressure condition, applying a very high surface pressure may constrain the cleaning action of the drag removal force of the fluid flow. Therefore, the rock-cutter interface would again be affected by the confinement of the cutting flow. In other words, even though the increase in the fluid flow velocity can apply a higher drag removal force, the resultant surface pressure keeps the cuttings in the zone of penetration. Therefore, there are optimum conditions for the nozzle velocity, which the drag force overcomes the surface pressure.

Taking into account the above indicated concepts, it can also be speculated that there is even still a better situation for applying the hydraulic power on the zone of penetration as one of the effective means for achieving a better bit performance under an elevated borehole pressure. The bit hydraulics should be optimized with respect to the specific conditions of a drilling operation such as BHP, rock type, rotary speed and WOB, with which by applying the minimum required jet velocity and maximum flow rate the maximum cleaning capacity with less rock strengthening would be achieved. The role of instant cleaning of the cuttings can be more influential, especially when the bit penetrates a rock with higher DOC, and when there are regions far from the high velocity of a jet flow.

The available hydraulic power of a pump can be spent on injection of a certain amount of flow rate with a specific jet velocity. These two parameters can be kept in an optimized balance by selecting an appropriate nozzle size. This means that, by keeping

the nozzle velocity at an optimized value, the total flow rate becomes maximum, in which the regions far from the direction of the jet flow becomes cleaned more effectively.

In order to simplify this optimization the following example is provided. For the pump system which is used in this experiment, it is assumed that all the hydraulic power of 20 kW is available. Also, it has been found that jet velocity of 62 m/s is sufficient for generation of an appropriate differential pressure for both BHPs of 1100 kPa and 2100 kPa. The relation of bit pressure drop and jet velocity is given by Equation (19) in SI units.

$$\Delta P_{\text{bit}} = \frac{\rho_m \times U_n^2}{C_d^2} \quad (23)$$

Therefore, applying the nozzle discharge coefficient of 0.7 and density 1000 kg/m³ for water, the bit pressure drop vs. velocity will be simplified to Equation (20) in SI units.

$$\Delta P_{\text{bit}} = 2040 U_n^2 \quad (24)$$

Therefore ΔP_{bit} of 7840 kPa is calculated for a jet flow velocity of 62 m/s. On the other hand the hydraulic power is given by Equation (21) in SI units.

$$\text{Pump power} = \Delta P_{\text{bit}} \times Q \quad (25)$$

The flow rate of $0.002551 \text{ m}^3/\text{s}$ or $150 \text{ L}/\text{min}$ is calculated for the assumed available hydraulic power.

As the flow rate and jet velocity are known, the optimized total flow area for this bit will be 41.145 mm^2 or two nozzles with diameters of 5.12 mm . In the other words, it is possible to have a better nozzle configuration for the bit which is used in this experiment.

Through the above indicated optimization a higher WOB can be applied to increase the depth of cut as the overall drag removal force is maximized with fulfillment of the optimum jet velocity.

The containment of cutting flow can also constrain the performance of roller cone bits. Figure 58 shows how BHP causes containment of the cutting flow in front of the tooth of a roller cone bit. In addition the generated cutting on the right hand side of the tooth, due to direct hold-down force of BHP and a poor bit hydraulic condition, remains in its place, and the bit will regrind it in the next actions under the severe condition of the cutting flow.

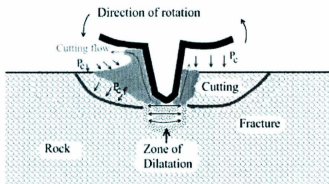


Figure 58. Containment of cutting flow under the tooth of a roller cone bit

The BHC is observed to have a limited influence on improvement of the drilling efficiency. The fluid flow cleans the generated cuttings on the top of the zone of the penetration. Therefore, complete elimination of the negative effect of the cutting flow on the rock strengthening, with current technology of drilling, based on the cleaning mechanism of the jet flow, is impossible. This phenomenon can be more problematic, under an elevated BHP when the cuttings are not able to jump out of the zone of the penetration before accumulation.

7. Results, Discussion and Analysis of Numerical Simulation *

7.1. Generation of Simulation Environment

In order to prepare the simulation environment, a rock-cutter interaction using distinct element method is developed. Figure 59 presents a schematic view of the components and conditions of the simulation.

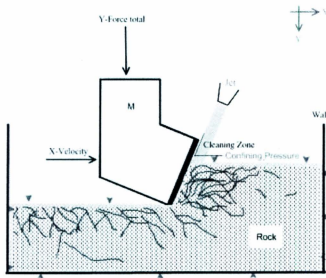


Figure 59. Conditions and components of the simulation

* This chapter has been published in the proceeding of 46th US Rock Mechanic and Geomechanic Symposium in June 2012, authored by Hossein Khorshidian, Mohammad Mozaffari and Stephen Butt. This chapter has been modified from the published paper by adding Figure 62 and 61 which assists with the analysis of the simulation results.

In the first step of the simulation, a rectangular rock block has been generated based on a DEM contact model which are supported by material genesis function in the library of PFC 2D [45].

A linear contact model is implemented between circular particles for generation of a two dimensional rock sample. The circular particles are considered a cylinder with the length of 1m for three dimensional evaluations. In the linear model, particles with a specific normal and shear stiffness are joined such as two springs in series. Also, the parallel bond and dashpot can be defined along abovementioned contact model. The parallel bonds play the role of cement between particles.

DEM parameters have been adjusted to match macro properties of Carthage Limestone which was obtained from calibration with real UCS tests [45, 46]. The rock sample was generated by defining normal and shear parallel bonds with strength of 91 MN between particles.

These particles constitute minimum diameter of 0.35 mm and density of 2620 kg/m³. In addition, the module of stiffness of the particles at their contacts is adjusted to 83 GPa, which in three dimensional system is proportional to the normal stiffness of particles. The ratio of the normal stiffness to the shear stiffness is 3.8. Also, the coefficient of friction between particles is set to 0.5.

The generated rock sample constitutes width of 250 mm and height of 30 mm. The local damping of the rock particles is 0.5, and both the normal and shear viscose damping of the contact are adjusted to 0.2. The surface of generated rock is opened for penetration, and the other sides are confined by fixed components which are called a wall. These walls

hold the specimen block from any significant motion during penetration of the cutter. The walls are 10% stiffer than the particles. Also, there is no bond and friction between the rock particles and walls.

In the second step of the simulation, a PDC cutter was simulated. The cutter constitutes fine particles (0.2 mm) with a stiffness and bond strength 100 times stronger than the rock sample and the same coefficient of friction. The cutter has back-rake angle is 20° and wear flat is 0.5 mm.

In the third step of the simulation, the hydrostatic confining pressure is applied on the rock block. The confining pressure can be applied by a force normal to the contact plane between particles which surround the rock. This pressure is fixed to 6800 kPa (1000 Psi) for the entire test. The applied confining pressure is acting on surface and right side of the rock. Therefore, the rock will be confined by the chain of applied pressure and the walls in the other sides. Through this method, the rock will be both pressurized and hold in its place during penetration.

In the next step, a cleaning condition was applied for removing the generated cuttings material during penetration. In the application of the cutter cleaning condition it is assumed that a fluid flow can remove the cutting material when the PDC cutter moves them up to 0.5mm above the surface of the rock.

The effect of gravity was also set to zero. Therefore, the value of load on the cutter will be fixed by changing the mass of the cutter, which represents the inertia of a BHA on top of a bit.

The cutter starts penetrating the rock by applying a vertical force in direction of “Y” axis and a horizontal velocity in direction of “X” axis (Figure 1). The particles which are used for applying the confining pressure are shown by a different color around the rock specimen. Also, the described cleaned zone is shown in front of the cutter with specified distance to the surface of the rock.

7.2. Testing Parameters and Data Analysis

In order to study the effect of cutter oscillation on penetration responses, the mass of the cutter, vertical load on the cutter and horizontal velocity of the cutter are considered as variable parameters, which were varied over three levels. The selected levels for the mass of the cutter are 2, 11 and 20 T (1 T = 1000 kg), which can be defined by adjusting the density of the particles in the cutter. Levels for the vertical load are 100, 125 and 150 kN, and for horizontal speed (V_x) are 0.5, 1 and 1.5 m/s.

The response of the simulation are the “X” and “Y” position of the tip of the cutter, vertical and horizontal force components in the cutter vs. time (t). In the analysis of the results it was assumed that the simulated components are extruded 1 m toward third axis which is not visible in the two dimensional simulation. This length is considered for all evaluations of the test responses.

The analysis of data is performed in regions of each test where the cutter stabilizes in its vertical position, and the DOC starts maintaining at a near constant value. The end of this region is 30 mm away from the wall in the right side of rock. This distance is sufficient for a normal chip generation and avoiding edge effects. Penetration near the rock boundary may generate a large chip with near horizontal shear plane and

accompanied by upward movement of the cutter or a high horizontal force. Figure 60 shows a region of study in a single cutter test. It can be seen that DOC of the cutter began to increase from the start of penetration and because of equilibrium in the force components acting on cutter, reached to a stabilized condition.

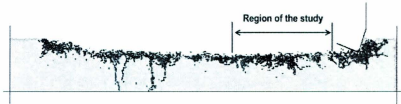


Figure 60. Region of study in a simulation of single cutter-rock interaction

In order to evaluate the performance of the cutter, MSE of the penetration was computed by Equation (22). The calculated MSE shows the amount of mechanical work of the horizontal force in front the cutter for removing a unit volume of the rock. In this equation “ F_x ” is the horizontal force in front face of the cutter, “ Y ” is the DOC and “ ΔX ” is the cutter advancement in each time step of the simulation. Also, “ t_1 ” and “ t_2 ” are the start and end of the time in the region of the study.

$$MSE = \frac{\sum_{t_1}^{t_2} (F_x \times \Delta X)}{\sum_{t_1}^{t_2} (Y \times \Delta X)} \quad (26)$$

7.3. Results and Discussion of Simulation Test

Table 6 shows results of the 27 simulation runs at specified levels of the studied factors. The first column shows the horizontal velocity of the cutter, and the second column shows the mass of the cutter at the three specified levels. The DOC and MSE of the cutter are shown in front of each specified level of vertical load.

Table 6. Results of simulation test

H. Vel. (m/s)	Mass (T)	Load (kN)	MSE (MPa)	DOC (mm)	Load (kN)	MSE (MPa)	DOC (mm)	Load (kN)	MSE (MPa)	DOC (mm)
0.5	2	100	22.05	7.999	125	24.06	9.437	150	26.01	10.27
0.5	11	100	17.55	7.172	125	22.25	8.455	150	23.66	9.758
0.5	20	100	18.98	8.322	125	22.32	8.534	150	24.22	9.364
1	2	100	18.18	5.822	125	23.93	7.515	150	26.63	8.461
1	11	100	27.6	6.407	125	27.11	6.827	150	29.77	8.32
1	20	100	17.46	5.712	125	20.51	8.796	150	31.84	9.385
1.5	2	100	26.08	4.478	125	26.35	6.283	150	32.65	7.739
1.5	11	100	27.95	7.572	125	28.51	6.107	150	35.17	7.916
1.5	20	100	25.1	4.357	125	32.66	6.22	150	37.34	8.811

The DOC is negatively influenced by increasing the horizontal speed of the cutter and decreasing the vertical load on the cutter. However, the mass of the cutter showed no significant influence on DOC. Therefore, average of DOC for three levels of the mass of the cutter at each specific level of load on the cutter and horizontal speed has been calculated to study the influence of the other factors on the drilling response. Figure 61 shows this average of DOC vs. load on the cutter at three levels of horizontal speed. It can be seen that increase in load increases the DOC, and increase in horizontal speed decreases the DOC. On the other hand, MSE is significantly affected by all the test factors.

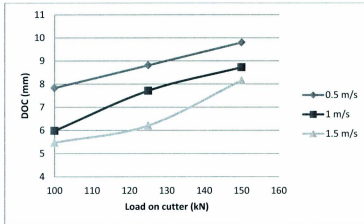


Figure 61. DOC vs. load on cutter and horizontal speed

In order to show the influence of WOB and horizontal speed on MSE, the average of MSE, for three levels of the mass of the cutter, vs. load on the cutter and horizontal speed is shown in figure 62. Increase in both load and horizontal speed increase the MSE.

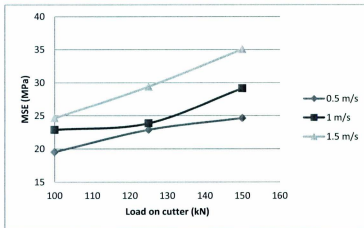


Figure 62. MSE vs. load on cutter and horizontal speed

The result of the MSE by a polynomial equation is correlated to the all factors of the test.

Equation (23) shows the achieved correlation in SI units.

$$\begin{aligned} \text{MSE} = & 2.571 + 0.147 \times F_y \\ & + 4.471 \times V_x - 0.00028 \times M \\ & + 0.307 \times (M \times V_x) \end{aligned} \quad (27)$$

Where, F_y is the vertical load on the cutter, M is mass of the cutter and V_x is the horizontal speed of the cutter. Figure 61 also presents the predicted MSE vs. actual value for this correlation.

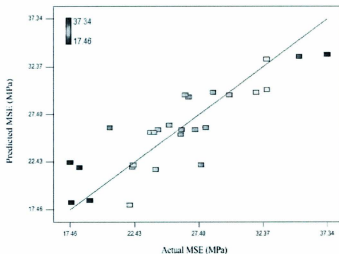


Figure 63. Predicted MSE in equation 23 vs. actual MSE

The correlation indicates that despite applying a cutter cleaning condition, increase in the load on cutter yields an increase in the value of MSE. This can be related to an insufficient applied cleaning condition. In this condition the containment of the cutting flow of generated fragments under the specific back-rake angle of the cutter applies an extra confinement on the rock surface in the zone of the penetration.

Figure 62 show the MSE vs. mass of the cutter and horizontal velocity, and Figure 63 shows the contour plot of the three dimensional curve.

Equation (23), Figure 64 and Figure 65 imply that increase in the mass of cutter at low cutter horizontal velocity results in a lower MSE. Additionally, at the entire cutter masses, increase in horizontal speed will increase the MSE. However, at higher horizontal speeds, lowering the mass of cutter decreases the MSE value.

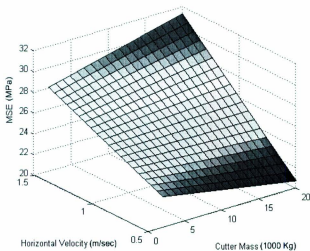


Figure 64. MSE vs. mass of the cutter and horizontal speed of cutter at load on cutter of 125 kN

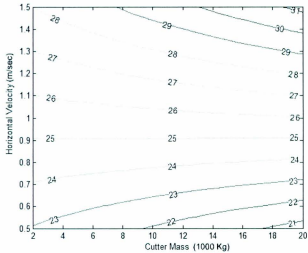


Figure 65. Contour plot of MSE vs. mass of the cutter and horizontal speed of cutter

The horizontal motion of the cutter during cutting actions is accompanied by vertical oscillations. The oscillations can be observed in the vertical position, vertical velocity and force components of the cutter.

The vertical vibration of the cutter is mainly related to the accumulation of particles between the cutter and the orientation of the resultant ramp after crushing the shear plane. This condition is depicted in Figure 66.

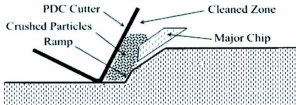


Figure 66. Sliding of PDC cutter on the rock surface

Those generated particles, which are held down by a confining pressure, may cause the cutter to move upward, as the cutter is no longer able to generate a new chip. The cutter can again move downward as another chip will be generated or when the upward force becomes less than the vertical load on cutter.

In order to investigate the effect of the cutter mass and horizontal velocity on the above indicated oscillations, the spectrums of the vertical velocity of the cutter and components of force in the front face of the cutter, have been studied. The results of the spectral analysis are shown for all levels of the cutter mass, high and low levels of the cutter horizontal velocity and vertical load of 125 kN. The selected levels properly represent the significance of entire test analysis. Figure 67 and 68 show the spectral analysis for the cutter vertical velocity in the high and low horizontal speed respectively. These figures present that the peak amplitude of the vertical velocity is higher for lower mass of the cutter. When the cutter constitutes a lower mass inertia, the vertical load on cutter and vertical force resulting from cutting action can excite the cutter with greater acceleration. Therefore, the velocity amplitudes in lower mass conditions constitute higher peaks.

Figure 69 and 70 show the spectrum of vertical force component in the front face of the cutter. These figures imply that the amplitudes of vertical force of the cutter for a lower mass condition constitute greater peaks. Also, the amplitudes have higher peaks at higher horizontal velocities.

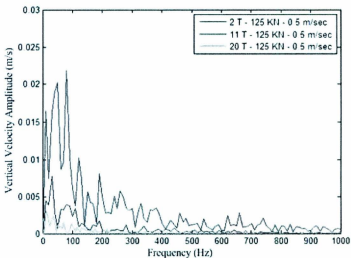


Figure 67. Spectrum of vertical velocity at horizontal speed of 0.5 m/s and vertical load of 125 kN

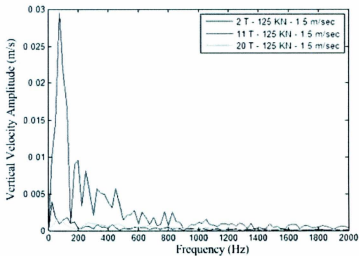


Figure 68. Spectrum of vertical velocity at horizontal speed of 1.5 m/s and vertical load of 125 kN

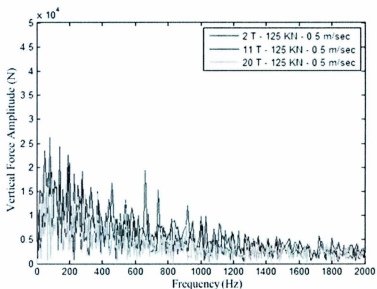


Figure 69. Spectrum of vertical force at horizontal speed of 0.5 m/s and vertical load of 125 kN

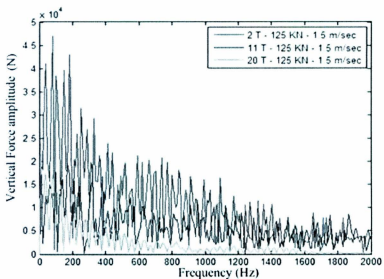


Figure 70. Spectrum of vertical force at horizontal speed of 1.5 m/s and vertical load of 125 kN

Moreover, the spectral analysis of the horizontal force in the front face of the cutter is presented in Figure 71 and 72. The analysis shows that at low horizontal velocity, the lower cutter mass results in higher horizontal force amplitudes, but at high horizontal velocity the lower cutter mass results in lower horizontal force amplitudes. The scenarios which result in higher amplitudes of the horizontal force may yield higher magnitudes of torque in the BHA of a rotary drilling system.

The aforementioned results indicate that the peak amplitudes of the vertical velocity of cutter are linked to the mass of the cutter. In order to discover the relation between MSE and vibration, the peak amplitude of vertical velocity, which is the response of tests, was applied as a factor in a new analysis. The modified polynomial correlation between MSE and peak amplitude of the cutter vertical velocity, V_y , horizontal velocity, V_x , vertical load on the cutter, F_y , is shown in Equation (24) in SI units. It can be seen that mass of the cutter showed no significance in the modified correlation, and the role of mass is rendered to the amplitude of the vertical velocity of the cutter (V_y). Figure 73 presents the predicted MSE of the new correlation vs. actual MSE of the test. In this figure it can be seen that MSE poses a better correlation to vertical velocity peak amplitude than to mass of the cutter.

$$\begin{aligned}
 \text{MSE} = & -1.923 + 0.147 \times F_y \\
 & + 11.034 \times V_x - 34.793 V_y \\
 & -479.566 \times (V_x \times V_y) + 17894.5 V_y^2
 \end{aligned} \tag{28}$$

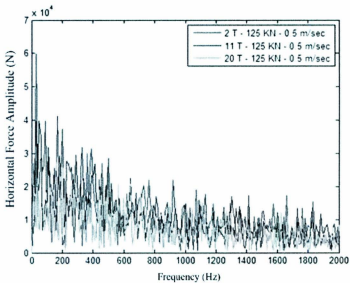


Figure 71. Spectrum of horizontal force at horizontal speed of 0.5 m/s and vertical load of 125 kN

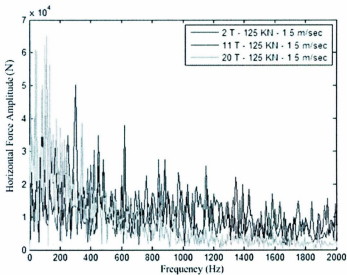


Figure 72. Spectrum of horizontal force at horizontal speed of 1.5 m/s and vertical load of 125 kN

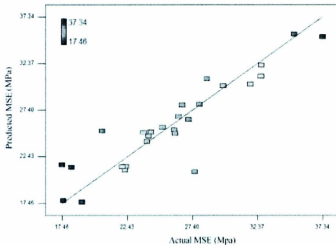


Figure 73. Predicted MSE in equation 24 vs. actual MSE

Figure 74 shows MSE vs. the cutter horizontal velocity and peak amplitude of the cutter vertical velocity in a 3D plot at the vertical load of 125 kN. Figure 75 also shows the contour plot of MSE vs. aforementioned factors. The modified MSE correlation implies that improvement in cutter performance can be achieved by optimizing the cutter vertical oscillation with respect to the cutter horizontal speed.

In drilling operations, the higher rotary speed is a potential factor for achieving higher rate of penetration (ROP). Although Table 6 shows that at a higher horizontal velocity of cutter the DOC will be decreased, in rotary drilling, due to successive cutting actions, a higher ROP may be achieved at higher rotary speeds. Moreover, an appropriate oscillation of vertical velocity of the cutter can mitigate increase of MSE at higher rotary speeds. For example, Figure 75 shows that at a horizontal speed of 1.5 m/s, increase in

peak amplitude of the vertical velocity via adjusting the mass of the cutter can reduce the MSE from 32 MPa to 25 MPa.

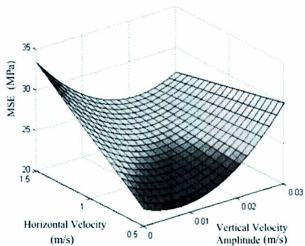


Figure 74. Curve of MSE vs. horizontal velocity and peak of the axial velocity amplitude of cutter

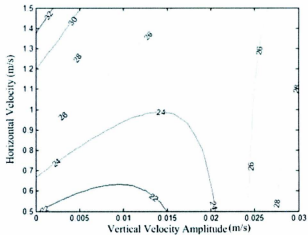


Figure 75. Contour plot of MSE vs. horizontal velocity and peak of the axial velocity amplitudes

Spectral analysis of the cutter vertical position in the same levels of the aforementioned analysis is depicted in Figure 76 and 77.

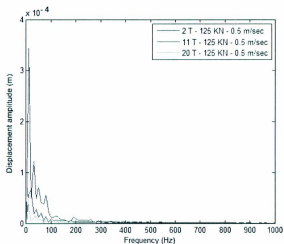


Figure 76. Spectrum of cutter vertical position at speed of 0.5 m/s and vertical load of 125 kN

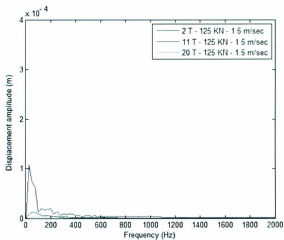


Figure 77. Spectrum of cutter vertical position at speed of 1.5 m/s and vertical load of 125 kN

It can be seen that the peak of the displacement amplitude of the cutter for a low mass condition is higher than a heavier mass. Also, this value is significantly larger at low horizontal velocity. The reason of decrease in the amplitude of the cutter vertical displacement in the high horizontal velocity might be due to a high horizontal inertia of the cutter. Thus, the heavier cutter tends to stay at the direction of cut with a low vertical displacement. Consequently, in this condition the amplitudes of the horizontal force component will be larger when the cutter is not able to generate chips. In this condition, the cutter may crush the rock instead of moving upward. On the other hand, decreasing the cutter mass at the high speed eases its vertical movement which in addition to decreasing the horizontal force component, applies impacts on the cutter-rock interface.

Based on the achieved results it is speculated that there are two signs for influence of the cutter vertical vibration on penetration mechanism. The positive effect can be significant when the cutter imposes a sufficient impact on the rock for cratering. In other words, the impacts with low energy create no damage on the rock. On the other hand, the correlation shows that exceeding the optimal point of vibration will increase the MSE.

The vertical velocity amplitude and vertical displacement amplitude are linked to each other. Therefore, higher vertical velocity amplitudes results in higher displacement amplitudes. However, excessive fluctuations in vertical position of the cutter can result in no penetration in direction of the cut. In other words, the cutter tends to slide on the ramp instead of chipping or crushing. Therefore, there is an optimal condition for vertical oscillations condition which should be controlled with respect to the other drilling parameters such as the horizontal velocity and rock strength.

The main reasons of the improvement in the penetration mechanism of the PDC cutter due to vertical oscillation are both the decrease in the required horizontal force for cutter advancement and the generation of larger chips after imposing an energized impact. As the cutter vertical fluctuations exist for all horizontal motions, a cutter with a lower inertia consumes less energy for axial oscillations. Additionally, those impacts assist the cutter in generation of larger chips and craters.

Figure 77 shows the generation of the cutting in front of the PDC cutter under a low vertical force oscillation condition, which represents normal chipping. Figure 79 shows the generation of the cutting under a high vertical force oscillation condition. The shape of the chip is similar to craters which a wedge may generate on rock surface after an impact. In Figure 79, the vertical crack underneath the cutter is due to applying a high energy impact to the rock. In addition to above circumstances, it is speculated that in the case of a lower inertia, the cutter applies a lower confinement on the rock. This confinement is due to accumulation of crushed particles between the rock and cutter with specific back-rake angle.

Of course, it is important that cutter vertical vibrations would be able to generate significant cracks in the rock. Otherwise, the vibration only shows a negative effect on cutter performance, which has been observed at low horizontal speed of the cutter.

The effect of cutter vertical oscillation on the penetration mechanism can be dependent on drilling conditions such as rock strength, rock elasticity, bottom-hole pressure, cutter geometry, DOC, bit wear and specifically, the drill string stiffness.

Therefore, by considering all conditions of a drilling operation, optimizing the vertical oscillations can provide enhancements in the performance of PDC bits.

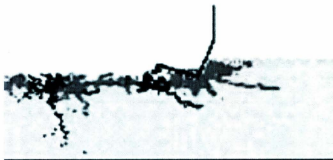


Figure 78. Normal chipping in front of PDC cutter

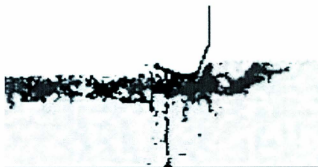


Figure 79. Combination of chipping and cratering after impact of PDC cutter

8. Future Work

The experimental results show that the main factors reducing ROP under elevated borehole pressure is not only the influence of the hydrostatic pressure on rock failure, but is containment of the flow of crushed cuttings between the cutter and rock interface. Thus, the key to improvement in bit performance is cleaning of the fragments and crushed material. In addition, it has been observed that utilizing a bit with a high power jet, despite significant mitigation in cleaning of the generated rock cuttings, is not able to bring the penetration operation to a desirable condition. Therefore, novel methods, e.g. administering vibratory cleaning and new design of the bit, should be considered for achieving a better drilling efficiency.

Results of the simulation test shows agreements of DEM with realistic penetration phenomena, e.g., properties of the shear plane, ribbon shape cuttings material and dynamic motion of the cutter. However, DEM still suffers from lack of fit in amount of DOC and MSE with experimental data. The achieved DOC is higher and MSE is lower than experimental results [13]. Therefore, further improvement is required for a rock distinct element contact model which accounts for compliance at the rock-bit contact. Additionally, the current DEM model of the specimen contains particles with minimum diameter of 0.35 mm. Therefore, the simulation of fine particles in between the cutter and rock is limited to large sizes and smaller sizes should be considered in future works.

9. Conclusions

Through the experimental study it is found that the performance of a bit in the penetration of rock is significantly reduced under elevated borehole pressure. Analysis of MSE shows that although under negligible BHP, minimum MSE is still considerably higher than rock strength, increase in BHP increases the MSE value unexpectedly. Analysis of rock-cutter interaction showed the dominant role of the containment of cutting flow in the confinement of the rock surface in the zone of penetration during drilling. The accumulation of cuttings, and consequently the intensity of cutting flow, is more problematic under the hold-down force of borehole pressure.

The resultant friction, due to cutting flow in front of the cutter face, is the function of cutter geometry and the coefficient of friction between the cutter and drilled particles.

Moreover, administering a jet flow can mitigate the bit performance by removing the cuttings. The jet flow applies two types of forces on the particles. The first type is a drag force, and the second type is a hold-down force. Therefore, there is an optimum condition for applying a high velocity jet flow on the zone of penetration with respect to the conditions of drilling in which the overall drag force becomes greater than hold-down force due to direct jet impingement.

In addition, the simulation of a single PDC cutter-rock interaction and analysis of cutter dynamics, show that the mass of the cutter in penetration of a rock is a significant factor which influences the MSE of drilling. Decreasing the mass of the cutter, under a fixed vertical load, causes significant vertical oscillations. The source of excitation is the horizontal force on the cutter which pushes the cutter upward in the generated ramp of the

120

rock-cutter interface. These vertical oscillations cause the cutter to impact on the rock when the cutter edge reaches the rock surface. Furthermore, the impacts of the cutter can be stronger when the cutter moves with higher vertical velocity amplitudes and horizontal speeds.

It has been also found that the negative effect of cutter vibrations can be due to the fluctuations in the cutter vertical position, and the positive effect of vibrations is related to those impacts that are sufficiently powered for creating significant damage on the rock surface.

References

1. A.T. Bourgoyne, K.K. Millheim, M.E. Chenevert and F.S. Young. (1991). "Rotary Drilling Process" in *Applied Drilling Engineering*. Richardson: SPE.
2. Garnier, A. J. and Van Lingen, N. H. (1959). Phenomena Affecting Drilling Rates at Depth. *Petroleum Transaction, AIME*, 216, 232-239; *SPE*, (1097-G).
3. Rafatian, N. (2006). *Effect of Pore Pressure on Single Cutter Forces*. (Master's research proposal). The University of Tulsa, Tulsa.
4. Teale, R. (1965). The Concept of Specific Energy in Rock Drilling. *Intl. J. Rock Mech. Mining Sci.*, 2, 53-57.
5. Caicedo, H. U., Calhoun, W. M., & Ewy, R. T. (2005). Unique ROP Predictor Using Bit specific Coefficient of Sliding Friction and Mechanical Efficiency as a Function of Confined Compressive Strength Impacts Drilling Performance. *Amsterdam, Netherlands: 2005. SPE/IADC Drilling Conference*.
6. Pessier, R., & Damschen, M. (2011). Hybrid Bits Offer Distinct Advantages in Selected Roller-Cone and PDC-Bit Applications. *SPE Drilling & Completion*, 26(1).

7. Tutluoglu, Levent. 1984. *Mechanical rockcutting with and without high pressure water jets*. University Microfilms International, Ann Arbor, MI. PhD dissertation, University of California, Berkeley.
8. Rittinger, P. (1867). *Von Lehrbuch Der Aufbereitungskunde*, Berlin, Ernst and Korn.
9. Cook, N.G.W. and Joughin, N.C. (1970). Rock Fragmentation by Mechanical, hemical and Thermal Means, *Proceedings of the 6th International Mining congress, Madrid, Paper 1- C.6*.
10. Maurer, W. (1965). Bit-Tooth Penetration Under Simulated Borehole Conditions. *JPT*, 1433-1442; *SPE*, (1260).
11. A.T. Bourgoyne, K.K. Millheim, M.E. Chenevert and F.S. Young. (1991). "Drilling Hydraulics" in *Applied Drilling Engineering*. Richardson: SPE.
12. Thomson, I. J., Krasuk, R. M., Silva, N., & Romero, K. (2011). Hybrid Drill Bit Improves Drilling Performance in Heterogeneous Formations in Brazil. *Brazil Offshore. Macaã*©, Brazil: Society of Petroleum Engineers.

13. Rafatian, N., Miska, S., Ledgerwood, L. W., Ahmed, R., Yu, M. and Takach, N. (2010). Experimental Study of MSE of a Single PDC cutter Under Simulated Pressurized Conditions. *SPE Drilling and Completion*, (119302), 10-18.
14. Maurer, W. (1965). Shear Failure of Rock under Compression. *SPE Journal*, (1054), 167-176.
15. Cunningham, R. A. and Eenink, J. G. (1959). Laboratory Study of Effect of Overburden, Formation and Mud Column Pressures on Drilling Rate of Permeable Formations. *Petroleum Transaction AIME*, (217), 9-17.
16. Sellami, H. Fairhurst, C. Deliac, E. Delbast, B. (1989) The role of in-situ rock Stresses and mud pressure on the penetration rate of PDC bits. *Rock at Great Depth*, (9061919754), 769-779.
17. Yang, J. H. and Gray, K. E. (1967). Single-Blow Bit-Tooth Impact Test on Saturated Rocks under Confining Pressure: 2. Elevated Pore Pressure. *SPE*, (1702), 389-408.
18. Black, A. D., Dearing H. L. and Dibona B. G. (1985). Effect of Pore Pressure and Mud Filtration on Drilling Rate in a Permeable Sandstone. *JPT*, 1671-1681; *SPE*, (12117).

19. Peltier, B. and Atkinson, C. (1987). Dynamic Pore Pressure Ahead of the Bit. *SPE Drilling Engineering*, 351-358.
20. Detournay, E. and Atkinson, C. (1991). Influence of pore pressure on the drilling response of PDC bits. *Rock Mechanics as a Multidisciplinary Science, Reogiers, (906191194X)*, 539-547.
21. Detournay, E., & Tan, C. P. 2002. Dependence of Drilling Specific Energy on Bottom-Hole Pressure in Shales. *SPE/ISRM Rock Mechanics Conference, Irving, Texas: 2002., SPE Inc.*
22. Gray-Stephens, D., Cook, J. M., & Sheppard, M. C. (1994). Influence of Pore Pressure on Drilling Response in Hard Shales. *SPE Drilling & Completion, 9(4)*.
23. Van Lingen, N. H. (1962). Bottom Scavenging – A Major Factor Governing Penetration Rates at Depth. *JPT*, 187-196; *SPE*, (165).
24. Wells, M., Marvel, T., & Beuershausen, C. (2008). Bit Balling Mitigation in PDC Bit Design. IADC/SPE Asia Pacific Drilling Technology Conference and Exhibition. Jakarta, Indonesia: 2008, IADC/SPE Asia Pacific Drilling Technology Conference and Exhibition.

25. Rodtke, R. P. and Pain, D. D. (1985). Optimization of PDC Bit Hydraulics by Fluid Simulation. SPE Annual Technical Conference and Exhibition. Las Vegas, Nevada: 1985 Copyright 1985, Society of Petroleum Engineers.
26. Maurer, W. (1962). The Perfect-Cleaning Theory of Rotary Drilling. *JPT*, 1270-1274; *SPE*, (408).
27. Garner., N. E. (1967). Cutting Action of a Single Diamond Under Simulated Borehole Conditions. *Society of Petroleum Engineering*.
28. Tibbitts, G. A., Sandstrom, J. L., Black, A. D., & Green, S. J. (1981). Effects of Bit Hydraulics on Full-Scale Laboratory Drilled Shale. *SPE Journal of Petroleum Technology*, 33(7).
29. Cholet, H. J., Petrole, d. F., Abdullah, H. F. and Chia, W. K. (1987). Improved Hydraulics for Rock Bits With Extended Slant Nozzles. *SPE Annual Technical Conference and Exhibition. Dallas, Texas: 1987 Copyright 1987, Society of Petroleum Engineers*.
30. Feenstra, R. and Van Leuween, j.j. M. (1964). Full-Scale Experiments on Jets in Impermeable Rock Drilling. *Society of Petroleum Engineering*.

31. Ledgerwood, L.W., Salisbury, D.P. (1991). *Bit Balling and Wellbore Instability of Downhole Shales*. SPE Annual Technical Conference and Exhibition. Dallas, Texas: 1991 Copyright 1991, Society of Petroleum Engineers Inc.
32. Rabia, H. (1989). *Rig Hydraulics*. Newcastle: Entac Software. 156-158.
33. McLean, R. H., (1965). Velocities, Kinetic Energy and Shear in Crossflow Under Three-Cone Jet Bits. *Journal of Petroleum Technology*. 1443-48, *Trans. AIME* 234.
34. Eckle, J.R. (1968). Microbit Studies of the Effect of Fluid Properties And Hydraulics on Drilling Rate, II. *Society of Petroleum Engineering*.
35. Armenta, M. (2008). Identifying Inefficient Drilling Conditions Using Drilling Specific Energy. Presented at SPE annual technical conference and exhibition held in Denver, Colorado, USA, 21-24 Sep. 2008.
36. Leach, S. J. and Walker, G. I. (1966). The Application of High Speed Liquid Jets to cutting - Some aspects of rock cutting by high speed water jets. *Proceedings of the Royal Society of London, A*, vol. 260, pp. 295-308.

37. Speer, J. W. (1958). A Method for Determining Optimum Drilling Techniques. *Drilling and Production Practice. API, pp. 130-147.*
38. Aadnoy, B.S., Cooper, I., Miska, Z.S., Mitchel, R.F., and Payne, L. 2009. "Wellbore Measurement Tools, Techniques, and Interpretation" *In Advanced Drilling and Well Technology.* Texas: SPE, 544-556.
39. Akbari, B., Butt, S.D., Munaswamy, K., and Arvani, F. 2011. Dynamic Single PDC Cutter Rock Drilling Modeling And Simulations Focusing On Rate of Penetration Using Distinct Element Method. *45th U.S. Rock Mechanics / Geomechanics Symposium. San Francisco, California: American Rock Mechanics Association.*
40. Dunayevsky, VA., Abbasian, F., and Judzis, A. 1993. Dynamic Stability of Drillstring Under Fluctuating Weight on Bit. *SPEDC 8 (2): 84-92. SPE-14329-PA. DOI: 10.2118/14329-PA.*
41. Dubinsky, V.S.H., Henneuse, H.P., and Kirkman, M.A. 1992. Surface Monitoring of Downhole Vibrations. Russian, European, and American Approaches. Paper SPE 24969 presented at European Petroleum Conference, Cannes, France, 16-18 November. DOI: 10.2118/24969-MS.

42. Payne, M.L., Abbasian, F., and Hatch, A.J. 1995. Drilling Dynamic Problems and Solutions for Extended-Reach Operations. *In Drilling Technology PD-volume 65, ed. J.P. Vozniak, 191-203. New York: ASME.*
43. Richard, T., Detourmay, E., Fear, M., Miller, B., Clayton, R., & Matthews, O. 2002. Influence of bit-rock interaction on stick-slip vibrations of PDC bits. *SPE Annual Technical Conference and Exhibition. San Antonio, Texas: Copyright 2002, Society of Petroleum Engineers Inc.*
44. Matthias, R., G, H., P., & Friedhelm, M., 1995. Drilling Performance Improvements Using Downhole Thrusters. *SPE/IADC Drilling Conference. Amsterdam, Netherlands, SPE/IADC Drilling Conference.*
45. Itasca Consulting Group Inc. 2008. "Fish in PFC2D". *In Material Genesis Support. p 3.24-3.58.*
46. Emam, Sacha. and David Potyondy. 2010. Technical Memorandum. Internal Technical Memorandum - PFC2D Rock-Cutting Procedures.
47. ASTM Standard D7012–10, 2010, "Standard Test Method for Compressive Strength and Elastic Moduli of Intact Rock Core Specimen under Varying States

of Stress and Temperatures," ASTM International, West Conshohocken, PA,
2010, DOI: 10.1520/D7012-10, www.astm.org.

Appendix A: Petrographic Information of Aggregates in Rock Specimens

Table 7 shows the petrographic information of the aggregates which are used for preparation of rock specimens.

Table 7. Petrographic information of aggregates in rock specimen

Rock/Mineral Types	Total per sieve fraction (%)					
	5-2.5 mm	2.5-1.5 mm	1.25-0.63 mm	0.63-0.315 mm	0.315-0.16 mm	Weighted Content
	17.40%	19.10%	18.20%	18.30%	16.10%	-
Granit	80%	72%.5	27.40%	6.30%	0	38.10%
Volcanic	17.30%	8.40%	7.90%	1.20%	0.60%	7%
Quartz	1.40%	10%	34%	76.20%	86.40%	40.60%
Feldspar	0	8.20%	30%	12%	7.60%	11.70%
Biotite	0	0	0	2.80%	3.80%	1.30%
Weathered Particles	1.30%	0.90%	0.70%	1.50%	1.60%	1.20%
Total	100%	100%	100%	100%	100%	99.90%

Appendix B: Table of Experimental Results

The results of the tests which are MSE and ROP are shown in Table 8. The levels of test factors, which are BHP and flow rate, are indicated in the second and third column respectively. The ROP and MSE of the tests are shown in fourth and fifth column for each replication. The last columns indicate the averages ROP and MSE of four replications at specified levels of the test factors. Results of additional experiments at flow level of 142 L/min, which have been performed only at BHP of 1100 kPa and 2100 kPa with two replications, are shown below the main results. In addition, two single replication tests have been performed under atmospheric condition. In one of these tests no water flow is applied, and in the other air is used as a drilling fluid. The results of complementary tests are shown at the end of Table 8.

Table 8. Results of experiment

Test Number	BHP (kPa)	Flow Rate (L/min)	ROP (m/hr.)	MSE (MPa)	AVE. ROP (m/hr.)	AVE. MSE (MPa)
1	130	30	6.563	193.59	6.54	193.46
2			6.667	188.04		
3			6.606	186.84		
4			6.336	205.37		
5		58	7.848	167.44	7.71	164.11
6			8.215	163.19		
7			7.639	160.98		
8			7.142	164.85		
9		86	7.297	189.67	7.51	177.43
10			7.618	169.28		
11			7.715	164.75		
12			7.394	186.03		
13		114	7.168	183.09	7.44	170.69
14			7.776	173.11		
15			7.254	164.24		
16			7.582	162.32		

Test Number	BHP (kPa)	Flow Rate (L/min)	ROP (m/hr.)	MSE (MPa)	AVE. ROP (m/hr.)	AVE. MSE (MPa)
17	1100	30	6.102	194.04	5.76	215.2
18			6.322	206.22		
19			4.903	233.32		
20			5.706	227.2		
21		58	6.739	179.13	6.36	186.55
22			6.703	180.24		
23			6.325	192.6		
24			5.677	194.24		
25		86	6.642	193.8	6.42	182.93
26			6.509	179.62		
27			6.178	169.41		
28			6.35	188.91		
29	114	6.972	167.29	6.68	190	
30		6.804	200.35			
31		6.847	183.4			
32		6.113	208.97			

Test Number	BHP (kPa)	Flow Rate (L/min)	ROP (m/hr.)	MSE (MPa)	AVE. ROP (m/hr.)	AVE. MSE (MPa)
33	2100	30	4.849	235.4	5	220.4
34			5.252	200.94		
35			4.968	216.94		
36			4.936	228.3		
37		58	5.738	193.09	5.79	198.71
38			6.091	197.73		
39			5.954	187.6		
40			5.357	216.41		
41		86	6.293	188.53	5.95	202.69
42			6.242	195.36		
43			5.598	211.42		
44			5.656	215.46		
45		114	6.473	190.65	6.19	195.41
46			5.918	201.7		
47			6.084	195		
48			6.288	194.27		

Test Number	BHP (kPa)	Flow Rate (L/min)	ROP (m/hr.)	MSE (MPa)	AVE. ROP (m/hr.)	AVE. MSE (MPa)
49	1100	142	6.721	180.58	6.42	198.42
50			6.113	216.26		
51	2100		5.652	194.8	5.65	201.11
52			5.641	207.42		
53	0	0	5.634	193.54	5.634	195.54
53	0	Air	5.882	240.23	5.882	240.23



